JGR Atmospheres

RESEARCH ARTICLE
10.1029/2020JD033637

Uneven Warming Likely Contributed to Declining Near-Surface Wind Speeds in Northern China Between 1961 and 2016

Gangfeng Zhang[1,2,3], Cesar Azorin-Molina[3,4], Deliang Chen[3], Tim R. McVicar[5,6], Jose A. Guijarro[7], Feng Kong[8], Lorenzo Minola[3], Kaiqiang Deng[3], and Peijun Shi[1,2,9]

[1]State Key Laboratory of Earth Surface Processes and Resource Ecology, Beijing Normal University, Beijing, China, [2]Academy of Disaster Reduction and Emergency Management, Ministry of Emergency Management and Ministry of Education, Beijing Normal University, Beijing, China, [3]Regional Climate Group, Department of Earth Sciences, University of Gothenburg, Gothenburg, Sweden, [4]Centro de Investigaciones sobre Desertificación, Consejo Superior de Investigaciones Científicas (CIDE-CSIC), Moncada, Valencia, Spain, [5]CSIRO Land and Water, Canberra, ACT, Australia, [6]Australian Research Council Centre of Excellence for Climate Extremes, Canberra, ACT, Australia, [7]State Meteorological Agency (AEMET), Balearic Islands office, Palma, Spain, [8]College of Humanities and Development Studies, China Agricultural University, Beijing, China, [9]Key Laboratory of Environmental Change and Natural Disaster of Ministry of Education, Beijing Normal University, Beijing, China

Key Points:

- Homogenized wind speed has significantly ($p < 0.05$) declined over northern China, while it stabilized from the 1990s onwards
- Uneven warming has weakened meridional air temperature and pressure gradient, which has induced the slowdown of winds over northern China
- "All radiative" forcing can reproduce uneven warming and wind speed decreases, while they cannot be simulated by "natural-only" forcing

Supporting Information:

Supporting Information may be found in the online version of this article.

Correspondence to:

P. Shi,
spj@bnu.edu.cn

Citation:

Zhang, G., Azorin-Molina, C., Chen, D., McVicar, T. R., Guijarro, J. A., Kong, F., et al. (2021). Uneven warming likely contributed to declining near-surface wind speeds in northern China between 1961 and 2016. *Journal of Geophysical Research: Atmospheres*, *126*, e2020JD033637. https://doi.org/10.1029/2020JD033637

Received 4 AUG 2020
Accepted 3 MAY 2021

Abstract A decline in mean near-surface (10 m) wind speed has been widely reported for many land regions over recent decades, yet the underlying cause(s) remains uncertain. This study investigates changes in near-surface wind speed over northern China from 1961 to 2016, and analyzes the associated physical mechanisms using station observations, reanalysis products and model simulations from the Community Atmosphere Model version 5.1 (CAM5). The homogenized near-surface wind speed shows a significantly ($p < 0.05$) decline trend of −0.103 m s^{-1} decade^{-1}, which stabilized from the 1990s onwards. Similar negative trends are observed for all seasons, with the strongest trends occurring in the central and eastern parts of northern China. Fast warming has occurred at high-latitudes (i.e., >50°N) in recent decades, which has weakened the annual and seasonal meridional air temperature gradient (−0.33°C to −0.12°C dec^{-1}, $p < 0.05$, except autumn) between these regions (50°–60°N, 75°–135°E) and the northern China zone (35°–45°N, 75°–135°E). This caused a significant ($p < 0.05$) decrease in annual and seasonal pressure gradient (−0.43 to −0.20 hPa dec^{-1}) between the two zones, which contributed to the slowdown of winds. CAM5 simulations demonstrate that spatially uneven air temperature increases and near-surface wind speed decreases over northern China can be realistically reproduced using the so-called "all forcing" simulation, while the "natural only forcing" simulation fails to realistically simulate the uneven warming patterns and declines in near-surface wind speed over most of northern China, except for summer.

1. Introduction

Terrestrial near-surface wind speeds have declined over recent decades, showing a "stilling" trend (Roderick et al., 2007). This is particularly true for mid-latitude regions in countries such as Italy (Pirazzoli & Tomasin, 2003), Australia (McVicar et al., 2008), Canada (Wan et al., 2010), Spain and Portugal (Azorin-Molina et al., 2014), China (Shi et al., 2015) and many others (McVicar et al., 2012). The slowdown in near-surface wind speeds is associated with a widespread reduction in the number of dust storms (e.g., Wang et al., 2017) and weakened pan evaporation (e.g., McVicar et al., 2012). However, after 3–5 decades of a stilling trend in the average global terrestrial near-surface wind speed, the decline stabilized around 2013 and may have recovered slightly afterward (Azorin-Molina et al., 2019; Dunn et al., 2016; Tobin et al., 2014; Zeng et al., 2019). Regional wind studies have reported this recent rebound in land near-surface wind speeds for South Korea (Kim & Paik, 2015), Saudi Arabia (Azorin-Molina, et al., 2018) and China (Y. Li et al., 2018; R. Zhang et al., 2019). Zeng et al. (2019) reported that the stabilization occurred earlier in Asia (2001) and Europe (2003) than in North America (2012). The stilling and recent stabilization or slight recovery of near-surface wind speeds debate has highlighted an uncertainty in the assessment of long-term near-surface wind speed variability.

Declining near-surface wind speeds over the last 3–5 decades have helped alleviate soil wind erosion in arid and semi-arid areas throughout the world (e.g., southeast Spain (Segovia et al., 2017), northern China (G. Zhang et al., 2019); Central Asia (Li et al., 2020) and many others, and have mitigated wind-induced damage to infrastructure (Neumayer et al., 2014) and crops losses (Gardiner et al., 2016). However, weakened near-surface wind speeds have also reduced the diffusion of air pollutants to big cities and their long-distance transport (Cai et al., 2017; Lin et al., 2015), particularly in dry seasons when precipitation and therefore wet deposition are small. Shi et al. (2019) showed that weakening near-surface wind speeds in the lower troposphere accounted for 41.3% of the variance in the frequency of winter haze days for the Beijing-Tianjin-Hebei region between 1961 and 2014. Many countries, including China, Germany, and Denmark, view the exploitation of wind energy resources as key to meeting the reduced carbon emissions targets in the Paris Climate Accord (Peters et al., 2017; Rogelj et al., 2016). If the stilling trends in near-surface (i.e., 10 m) wind speed discussed above are also experienced to 250 m above the land surface (the upper height of wind turbine blades), then this suggests a reducing wind power potential and may present a challenge to the development of wind power generation. This is particularly true at mid-latitudes in the northern hemisphere, for which future climate projections have simulated decreases in wind power generation (Karnauskas et al., 2018).

Attribution of near-surface wind speed change is challenging as many factors drive wind variability (Azorin-Molina et al., 2018; Wu et al., 2018). Yet attribution improves our process understanding and informs debate over the recent stilling and/or recovery of near-surface wind speed trends. To explore the possible cause(s) of stilling, many have linked changes in wind speed to changes in large-scale atmospheric circulation (e.g., Azorin-Molina., et al., 2018; Belušić Vozila et al., 2019; Chen et al., 2013; Clifton & Lundquist, 2012; Minola et al., 2016). For example, Clifton and Lundquist (2012) concluded that the Arctic Oscillation (AO) explains 6% of near-surface wind speed changes in the state of Colorado in the United States. Chen et al. (2013) found that near-surface wind speed in China was much weaker for positive phases of El Niño–Southern Oscillation (ENSO), corresponding to warm sea surface temperatures (SSTs) in the Niño 3.4 region (5°S–5°N, 120°–170°W), than for negative phases, which correspond to cooler SSTs in the Niño 3.4 region. Minola et al. (2016) related decreases in near-surface wind speed in Sweden to a weakening of the North Atlantic Oscillation (NAO) between 1956 and 2013. Changes in large-scale atmospheric circulation indicate variations in regional pressure gradients, which are modified through thermal adaption in response to regional differences in warming (Lin et al., 2013).

Global near-surface air temperatures over land and sea increased rapidly during 1880–2012, with an average increase of 0.85°C (0.65°C–1.02°C), and the increase was particularly strong (0.12°C decade^{-1}) between 1951 and 2012 (IPCC, 2013). This recent warming trend evidenced striking spatial divergence, for example warming at high-latitudes (>50°N) in Eurasia was more rapid than at mid (30°–50°N) or low (0°–30°N) latitudes (Branković et al., 2012; Yao et al., 2017), reflecting the relatively weaker gradient in air temperature (and therefore in air pressure) between high- and mid- or low latitudes. Previous studies also demonstrated that global warming, driven by anthropogenic emissions, has changed global atmospheric circulation (Cai et al., 2015; Collins et al., 2010). For example, some studies have hypothesized that rapid warming of the Eurasian continent would weaken the large-scale meridional atmospheric flow from high-latitudes to mid- and low-latitudes, thus impacting wind dynamics over China (Y. Li et al., 2018; Lin et al., 2013). To more confidently attribute variability in near-surface wind speeds to spatially disparate warming patterns, studies using advanced model simulations of historical climate are needed. Climate models make attribution studies possible because the impact of potential drivers can be "isolated" with appropriately designed model simulations (Peng et al., 2018; Vautard et al., 2014).

The dominant near-surface wind speed trend over all of China has been negative since the 1960s (Lin et al., 2013; Shi et al., 2015), although the rate of decrease has lessened since around 1990 (R. Zhang et al., 2019). Winds in different regions of China are driven by varied atmospheric circulation systems, for example, near-surface wind speed in northern China is mainly modulated by the meridional pressure gradient (e.g., mid-latitude westerlies [Han et al., 2008] and East Asian winter monsoon [Wang et al., 2013]), while land-sea interaction (e.g., East Asian summer monsoon [Li et al., 2010]) is the primary driver of southern China near-surface wind speed. The spatially uneven warming over Eurasian discussed above modulates atmospheric circulation (Y. Li et al., 2018; Lin et al., 2013), for example by driving the formation

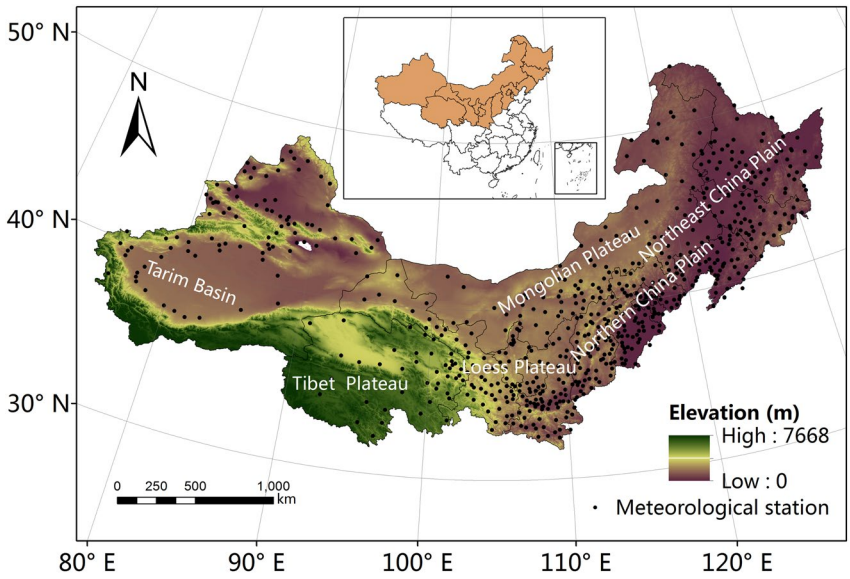

Figure 1. Terrain map showing the distribution of the 690 homogenized meteorological stations over northern China. Note that the white area at about 90°E and 42°N indicates Bosten Lake.

of high pressure anomalies over Mongolia and Siberia, which impacts near-surface wind speeds in northern China. Thus, northern China is selected in this study, which has a continental climate that varies from humid and semi-humid in the east to arid and semi-arid in the west. The main aim of this study is, therefore, to attribute changes in near-surface wind speed in northern China to spatial differences in warming over Eurasia using homogenized near-surface wind speed data sets, reanalysis products and model simulations of historical climate. The three objectives of this study are: (i) to investigate long-term trends and multi-decadal variability in annual and seasonal mean near-surface wind speeds, using homogenized near-surface wind speed datasets for northern China for 1961–2016; (ii) to explore the relationship between variations in near-surface wind speed and changes in near-surface air pressure and temperature; and (iii) to examine the drivers of the observed uneven warming distribution and attribute the observed near-surface wind speed trends for northern China to these drivers for the first time.

2. Data and Methods

2.1. Station Observations

Daily mean near-surface (10 m) near-surface wind speed was calculated from observations recorded four times daily between 20:00 and 20:00 the next day UTC, provided by the China Meteorological Administration (CMA; http://data.cma.cn/en, last accessed March 1, 2021). The raw near-surface wind speed data from 771 meteorological stations in northern China. Following Azorin-Molina et al. (2014), monthly mean near-surface wind speed was aggregated from the daily mean near-surface wind speed data at stations for which there were no more than five days of missing data in each month. Data were only used from stations for which monthly mean near-surface wind speeds were available for at least 99% of the 672 months between 1961 and 2016 (i.e., where there were fewer than 7 months of missing data over the 56 years). These conditions mean that data from 81 stations were excluded from our analysis. The spatial distribution of the 690 stations used herein is shown in Figure 1. Additionally, observed air temperature data from the Global Historical Climatology Network (https://www.ncdc.noaa.gov/data-access/land-based-station-data/land-based-datasets/global-historical-climatology-network-ghcn, last accessed March 1, 2021) were used, which consisted of 584 stations spanning 1961–2016 (see Figure S1).

Differences in anemometer height and type (Wan et al., 2010), anemometer aging (Azorin-Molina et al., 2018) and station location can artificially bias in-situ observations. For example, most meteorological stations use the EL-type cup anemometer that was adopted by the CMA in 1969, but at some stations this

was replaced with the EN-type cup anemometer in the early 1990s (Li et al., 2018). Also, not all 670 stations were equally active since 1961, with more wind data available in the recent decades (e.g., the 2010s) compared to early decades (e.g., the 1960s). Therefore, a homogenization protocol is necessary to correct artificial shifts and to infill missing data, thus creating a complete long-term data set. In this study, the 690 raw near-surface wind speed datasets and 584 raw air temperature datasets were homogenized using the well-established R software package Climatol (http://www.climatol.eu/; last accessed March 1, 2021; Guijarro, 2017), which has been successfully applied elsewhere (Azorin-Molina et al., 2016, 2018; Shi et al., 2019; G. Zhang et al., 2019). A detailed description of the homogenization method used here is provided in e.g., Azorin-Molina et al. (2016) and Shi et al. (2019).

2.2. Reanalysis Products

To investigate how air temperature and pressure gradients relate to near-surface wind speed trends and variability, monthly 10 m U and V wind (latitudinal and longitudinal wind in m s^{-1}), surface atmospheric pressure (hPa) and air temperature (°C, at ~2 m height) were downloaded from the National Center for Environmental Prediction, National Center for Atmospheric Research (NCEP–NCAR1 from 1961 to 2016, https://www.esrl.noaa.gov/psd/data/gridded/data.ncep.reanalysis.pressure.html; last accessed March 1, 2021; Kalnay et al. 1996). To compare with NCEP-NCAR1, surface pressure (hPa) and air temperature (°C, at ~2 m height) from ERA5 Reanalysis (https://cds.climate.copernicus.eu/, last accessed March 1, 2021; Hersbach et al., 2020), ERA-Interim Reanalysis (https://cds.climate.copernicus.eu/, last accessed March 1, 2020; Lindsay et al., 2014) and NCEP-NCAR 2 Reanalysis (https://psl.noaa.gov/data/gridded/data.ncep.reanalysis2.html, last accessed March 1, 2021; Kanamitsu et al., 2002) were also downloaded. These data have been widely used in studies of changes to atmospheric circulation in East Asia (e.g., Chen & Wang, 2015; Zhang et al., 2016). The extracted NCEP-NCAR1 products cover our study period (1961–2016) and are gridded with a horizontal resolution of 2.5° × 2.5°, while ERA5 (0.25° × 0.25°), ERA-Interim (0.75° × 0.75°) and NCEP-NCAR2 (2° × 2°) products are only available from 1979 to 2016. Reanalysis data covering the area bounded by 25°–65°N and 70°–140°E were examined here.

2.3. Climate Model Outputs

In addition to reanalysis datasets, daily surface air temperature (°C, ~2 m height), surface air pressure (hPa), 10 m U and V wind (m s^{-1}) were obtained from climate model outputs supplied by the Climate Variability Program (CLIVAR) Climate of the twentieth Century Plus Project (C20C+), part of the World Climate Research Program (http://portal.nersc.gov/c20c/main.html; last accessed March 1, 2021; Stone et al., 2019). In particular, the daily mean near-surface wind speed from reanalysis and climate model was calculated as $\sqrt{\left(u^2 + v^2\right)}$, following many existing studies (e.g., Minola et al., 2020; Shi et al., 2019). Here, these model data cover the area 25°–65°N and 70°–140°E. Two implementations of the Community Atmosphere Model version 5.1 (CAM5 atmosphere-only model) were used to calculate these historical simulations, both with horizontal resolutions of ~1° × 1°: (i) CAM5-All; and (ii) CAM5-Natural (hereafter CAM5-Nat). Simulations from both CAM5-All and CAM5-Nat have been widely used in climate change and attribution studies (e.g., Bellprat et al., 2019; Peng et al., 2018; Watanabe et al., 2014). Both CAM5-All and CAM5-Nat cover from January 1961 to December 2016 and each of the two experiments comprises 50 climate realizations, initialized from identical states except for a small perturbation to the three-dimensional temperature field. The CAM5-All simulations were driven by observed SST, sea ice conditions and historical greenhouse gas concentrations (the so-called "all forcing" simulation, Table 1). The CAM5-Nat simulations use the same solar irradiance, land cover and volcanic aerosol emissions as CAM5-All, but greenhouse gas emissions, tropospheric aerosol concentrations and stratospheric ozone levels are fixed at pre-industrial levels (the so-called "natural forcing" simulation). Note that anthropogenic contributions to SST and sea ice coverage were estimated from CMIP5 models and subtracted from present-day observation data to provide reasonable natural sea surface conditions for CAM5-Nat. Full details of the experimental design are available at the CLIVAR C20C1 Detection and Attribution Project website (http://portal.nersc.gov/c20c/main.html, last accessed March 1, 2021; Stone et al., 2019).

Table 1
Details of the CAM5.1 "all Forcing" (CAM5-All) and "Natural Forcing" (CAM5-Nat) Simulations From the CLIVAR C20C+ Detection and Attribution Project

Experiment information	CAM5-All	CAM5-Nat
Period	January 1961–December 2016	January 1961–December 2016
Number of realizations	50	50
Horizontal resolution	1° × 1°	1° × 1°
Greenhouse gases concentrations (ppm)	As observed	Pre-industrial
Sea surface temperatures (°C)	As observed	Anthropogenic attributable parts are subtracted
Sea ice conditions	As observed	Anthropogenic attributable parts are subtracted
Tropospheric aerosols	As observed	Pre-industrial
Volcanic aerosols	As observed	As observed
Solar irradiance (W/m^2)	As observed	As observed
Land cover	As observed	As observed
Stratospheric zone	As observed	Pre-industrial

2.4. Statistical Methods

We followed methods that have been successfully implemented previously to calculate long-term wind trends (Weatherhead et al., 1998). Near-surface wind speeds are considered in terms of anomalies, that is, as the deviation from the location-specific mean between 1981 and 2010, which prevents any particularly windy location from dominating the regional average near-surface wind speed. Trends in near-surface wind speed were calculated in meters per second per decade (hereafter m s^{-1} dec^{-1}) using Sen's slope method (Gilbert 1987), and an 11-year Gaussian low pass filter was used to assess multi-decadal near-surface wind speed variability. The statistical significance of the near-surface wind speed trends was calculated using Mann-Kendall's tau-b non-parametric correlation coefficient (Kendall & Gibbons 1990), and was expressed at three *p*-level thresholds (significant at $p < 0.05$, significant at $p < 0.10$, and not significant at $p < 0.10$, following McVicar et al., 2010; Minola et al., 2016; Zhang et al., 2020). The Pearson product-moment correlation coefficient (r) was used to assess the relationship between the wind anomalies and gradients in air temperature and pressure. Results were calculated separately for the boreal seasons: winter (December to February [DJF]), spring (March to May [MAM]), summer (June to August [JJA]), and autumn (September to November [SON]). According to Geostrophic Approximation Theory (Lin et al., 2013), near-surface wind speed variability over northern China may be explained by differences in near-surface air temperature and pressure between the high-latitude zone (50°–60°N) and the northern China zone (35°–45°N) both between 75°E and 135°E. Following previous studies (Y. Li et al., 2018; Zhang et al., 2020), the meridional air temperature and pressure gradient with respect to latitude was defined as:

$$SG = ABS\left[\frac{\sum_{i=1}^{n} CHL_i - \sum_{i=1}^{n} CNC_i}{n}\right] \quad (1)$$

where SG is the gradient in either air temperature (°C) or pressure (hPa); ABS means absolute value; n is the total number of grid cells at a given latitude; and CHL and CNC are the near-surface air temperature or pressure for grid cells in the high-latitude zone and the northern China zone, respectively.

To evaluate the reliability of NCEP-NCAR1, we also replicated the calculation of air temperature gradient using observed data from Global Historical Climatology Network. The variances explained by the regression between near-surface wind speed and air temperature as well as pressure gradient were calculated, to quantify to what extent the air temperature and pressure gradients explain the wind speed variability.

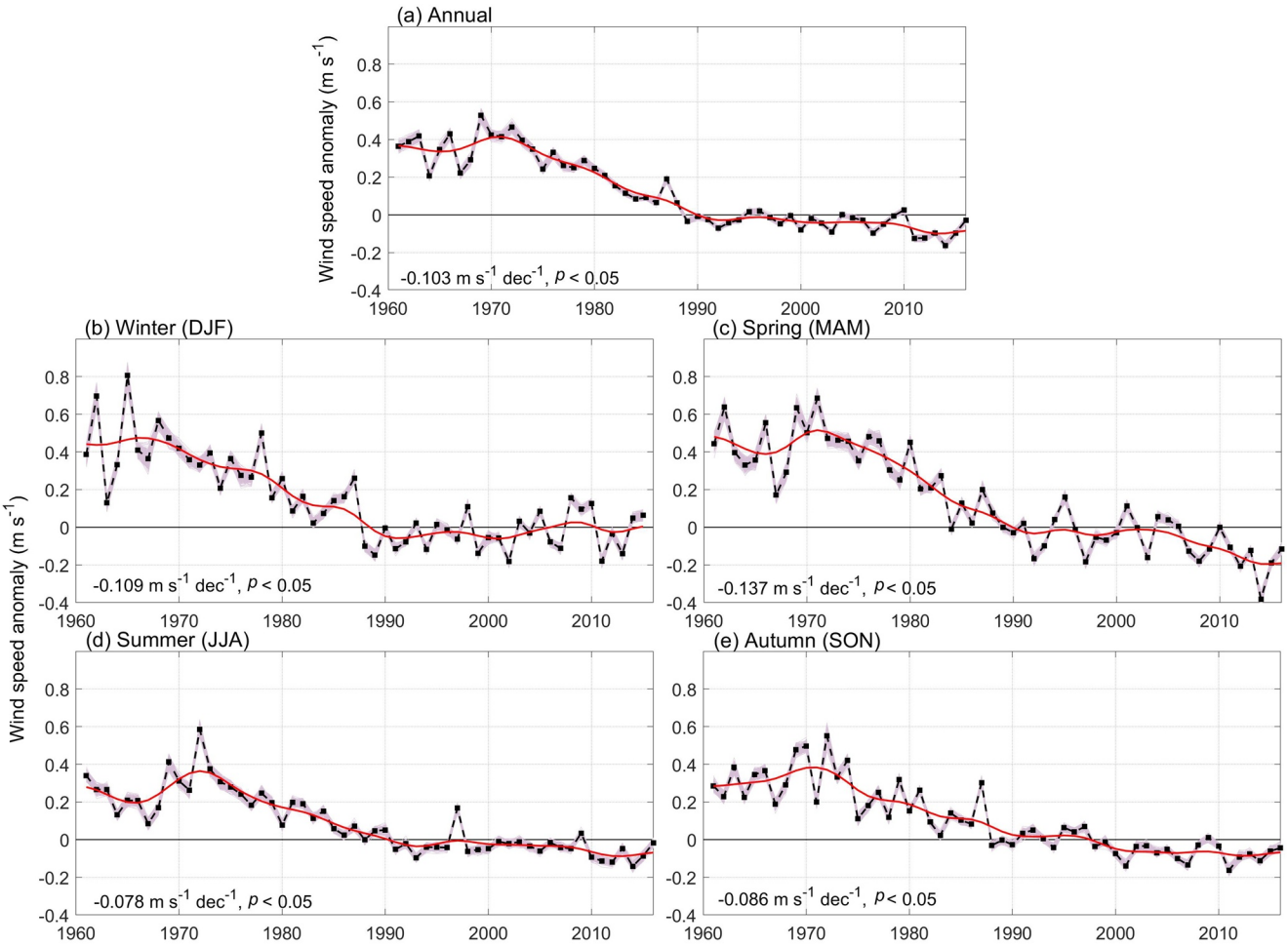

Figure 2. Annual and seasonal mean wind speed anomalies over northern China for 1961–2016. Wind speed anomalies of each station (in m s^{-1}) were calculated as the deviation from the 1981–2010 mean. Each pink line ($n = 400$) is a series for a randomly selected subset (40%) of the total stations over northern China. The red solid lines indicate the 11-year Gaussian low-pass filter. The magnitude (in m s^{-1} dec^{-1}) and statistical significance (p-level) of trends are also displayed for each plot.

3. Results

3.1. Near-Surface Wind Speed Trends Over Northern China

Figure 2 shows observed near-surface wind speed trends and variability over northern China from 1961 to 2016. The annual mean near-surface wind speed data have a significant ($p < 0.05$) negative trend of −0.103 m s^{-1} dec^{-1}, with seasonally averaged data also exhibiting a significant ($p < 0.05$) negative trend for all seasons. The strongest negative trend for the seasonally averaged data is for spring (−0.137 m s^{-1} dec^{-1}), followed by winter (−0.109 m s^{-1} dec^{-1}), autumn (−0.086 m s^{-1} dec^{-1}), and then summer, which experienced the weakest negative trend (−0.078 m s^{-1} dec^{-1}). After implementing the 11-year Gaussian low pass filter for the annually averaged near-surface wind speed data, three phases become apparent: (i) a stable phase from 1961 to 1970 with no positive or negative trend; (ii) a marked decreasing phase from 1971 to 1990; and (iii) a slightly more weakly decreasing, or possibly stable, phase from 1991. These three phases were also seen in the seasonally averaged data for every season except winter, where near-surface wind speeds began to recover slightly later in the third phase, from around 2000, see Figure 2. When looking stations comprising the eastern part of northern China (i.e., east of 100°E, 519 stations) and the western part of northern China (i.e., west of 100°E, 171 stations), both series showed similar multi-decadal variation (Figure S2). Furthermore, near-surface wind speed from NCEP-NCAR1 also displayed negative trends with a smaller magnitude (Figure S3), and significant ($p < 0.1$) trends were only found in summer and annually.

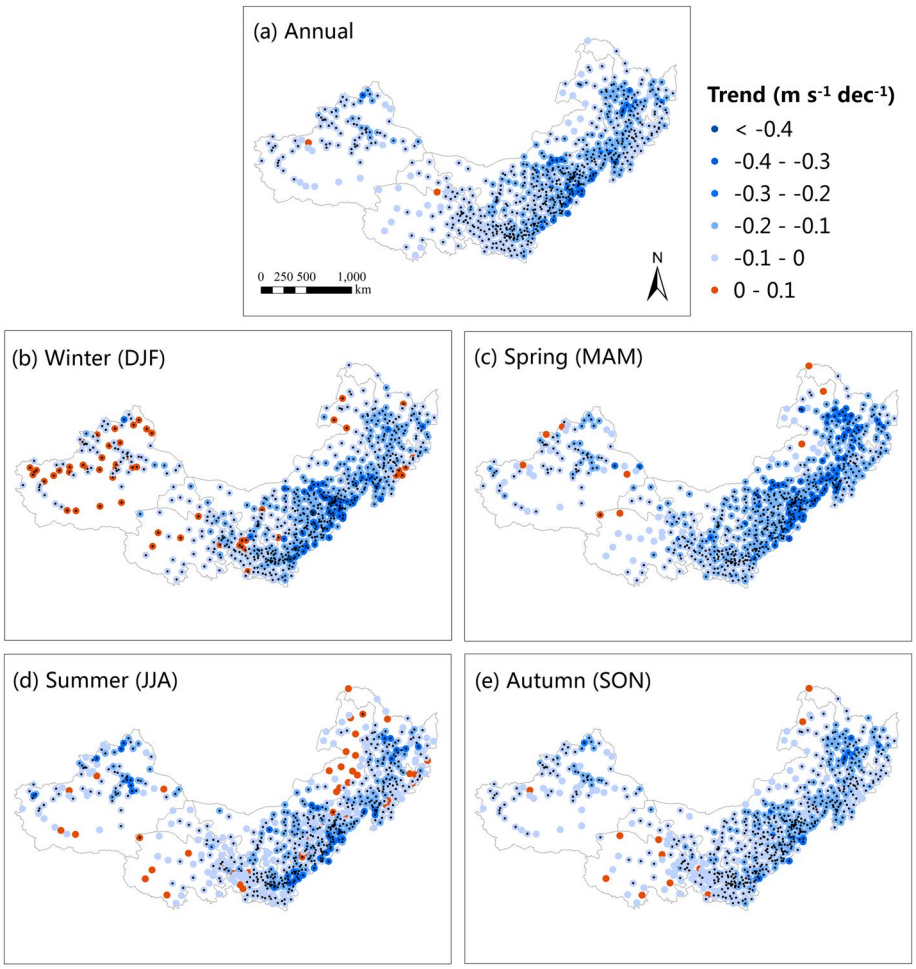

Figure 3. Spatial distribution of the sign and magnitude of annual and seasonal observed wind speed trends (in m s^{-1} dec^{-1}) over northern China for 1961–2016. The black dot in the circle represents a statistically significant trend at $p < 0.05$. The legend for part (a) applies to all other parts.

While a significant correlation between annual wind speed from station observations and NCEP-NCAR1 was found ($r = 0.49$, $p < 0.05$), the difference between trend and variability of wind speed from NCEP-NCAR1 and those from station observations might be to some extent due to the inclusion of satellite data in the assimilation process (Chen et al., 2013; Kalnay et al., 1996).

Figure 3 shows the spatial distribution of the trends in the annually and seasonally averaged near-surface wind speed data for northern China from 1961 to 2016, and Table 2 summarizes the relative frequency of stations having negative and positive trends at different significance levels. The dominant trend in annual near-surface wind speed over northern China is negative (recorded for 99.7% of stations), particularly over the Northern China Plains and Northeast China Plains (Figure 1). Most stations (>90%) are associated with a negative near-surface wind speed trend for all seasons, although this occurs less frequently for summer and winter than for spring and autumn. In winter, a negative trend was recorded at 91.9% of the stations, and was significant ($p < 0.05$) for 82.8% of the stations, with some stations in the northwestern part of the study area forming an exception. Most stations (98.7%) recorded negative trends in spring near-surface wind speeds with a stronger statistical significance than was associated with the winter trends, and these stations were mostly located in the middle and eastern parts of northern China. Some 93.3% of stations recorded negative near-surface wind speed trends for summer, and 80.1% of these trends were statistically significant (the lowest proportion of statistically significant trends for any of the four seasons). Some positive trends were recorded for summer near-surface wind speeds over parts of the Northeast China Plain and the Tibetan Plateau (corresponding to 6.7% of the stations). Autumn had the second highest proportion

Table 2
Percentage (%) of the 690 Stations With Significant (at $p < 0.05$ and $p < 0.10$) and Non-significant (at $p > 0.10$) Negative and Positive Trends in the Mean Observed Annual and Seasonal Near-Surface Wind Speed for 1961 to 2016

	Negative	Negative significant $p < 0.05$	Negative significant $p < 0.10$	Negative non-significant $p > 0.10$	Positive	Positive significant $p < 0.05$	Positive significant $p < 0.10$	Positive non-significant $p > 0.10$
Annual	99.7	95.2	96.8	3.2	0.3	0.0	0.0	100.0
Winter (DJF)	91.9	82.8	86.9	13.1	8.1	23.2	30.4	69.6
Spring (MAM)	98.7	93.2	94.9	5.1	1.3	11.1	11.1	88.9
Summer (JJA)	93.3	80.1	84.8	15.2	6.7	13.0	13.0	87.0
Autumn (SON)	98.4	87.3	90.3	9.7	1.6	0.0	9.1	90.9

of stations (98.4%) recording negative near-surface wind speed trends, particularly in the east of the study region; 87.3% of the stations recorded statistically significant decreasing trends in autumn near-surface wind speeds at $p < 0.05$ (Figure 3 and Table 2). Moreover, when looking at the spatial distribution of wind speed trends from NCEP-NCAR1 (Figure S4), it is quite different from widespread near-surface wind speed observed declines and features two different patterns: (i) widely significant negative trends in the north part of northern China and significant positive trend in the east part of northern China, in annual, winter, spring and autumn; and (ii) in summer widely significant increased wind speed in the north part of northern China, and nonsignificant wind speed changes in the east part of northern China.

3.2. Changes to the Near-Surface Air Temperature and Pressure Gradient and Their Effect on Near-Surface Wind Speed Variability

Figure 4 shows the spatial distribution of trends in annual and seasonal near-surface air temperature from NCEP-NCAR 1, and Figure 5 shows the temporal variability of the near-surface air temperature gradient between the high-latitude zone and the northern China zone from NCEP-NCAR 1. Annual air temperatures show significant ($p < 0.05$) warming trends, ranging from +0.20°C dec^{-1} to +0.60°C dec^{-1} in the high-latitude zone, while the northern China zone experienced smaller increases in air temperature, ranging from 0.00°C dec^{-1} to +0.40°C dec^{-1}; these were mainly concentrated in the eastern part of the study site where trends were statistically significant ($p < 0.05$). This spatially uneven warming pattern suggests a significant decrease in the air temperature gradient between the high-latitude zone and the northern China zone (−0.20°C dec^{-1}, $p < 0.05$), and a significant correlation ($r = 0.58$, $p < 0.05$, Table 3) was found between the near-surface wind speed anomalies here and the near-surface air temperature gradient.

Significant warming trends were found for winter in the middle and eastern parts of the high-latitude zone, and for eastern parts of the northern China zone (+0.30°C dec^{-1} to +0.60°C dec^{-1}, $p < 0.05$), while a slight cooling trend was found for winter in western parts of the northern China zone (−0.20°C dec^{-1} to 0.00°C dec^{-1}, $p > 0.05$). These changes combined give a significant decrease in the near-surface air temperature gradient, which is significantly correlated with the near-surface wind speed anomalies ($r = 0.38$, $p < 0.05$, Table 3). In spring, there were significant warming trends for the whole high-latitude zone (+0.30°C dec^{-1} to +0.60°C dec^{-1}, $p < 0.05$) and no significant warming trends for most of the northern China zone (0°C dec^{-1} to +0.20°C dec^{-1}, $p > 0.05$), while there was a slight cooling trend (−0.10°C dec^{-1} to 0°C dec^{-1}, $p > 0.05$) in the middle and north of the northern China zone. Overall, the near-surface air temperature gradient is associated with a significantly strong negative trend (−0.32°C dec^{-1}, $p < 0.05$), and correlates significantly and positively with the near-surface wind speed anomalies ($r = 0.57$, $p < 0.05$, Table 3). A similarly uneven warming pattern was found for summer, where the near-surface air temperature gradient had a significant negative trend (−0.24°C dec^{-1}, $p < 0.05$) and correlated significantly and positively with the near-surface wind speed anomalies ($r = 0.58$, $p < 0.05$, Table 3). Autumn warming trends were significant (+0.30°C dec^{-1} to +0.60°C dec^{-1}, $p < 0.05$) in the middle and western parts of the high-latitude zone, and were weaker, but significant, in western and eastern parts of the northern China zone (+0.20°C dec^{-1} to +0.40°C dec^{-1}, $p < 0.05$), while a slight cooling trend (−0.20°C dec^{-1} to 0°C dec^{-1},

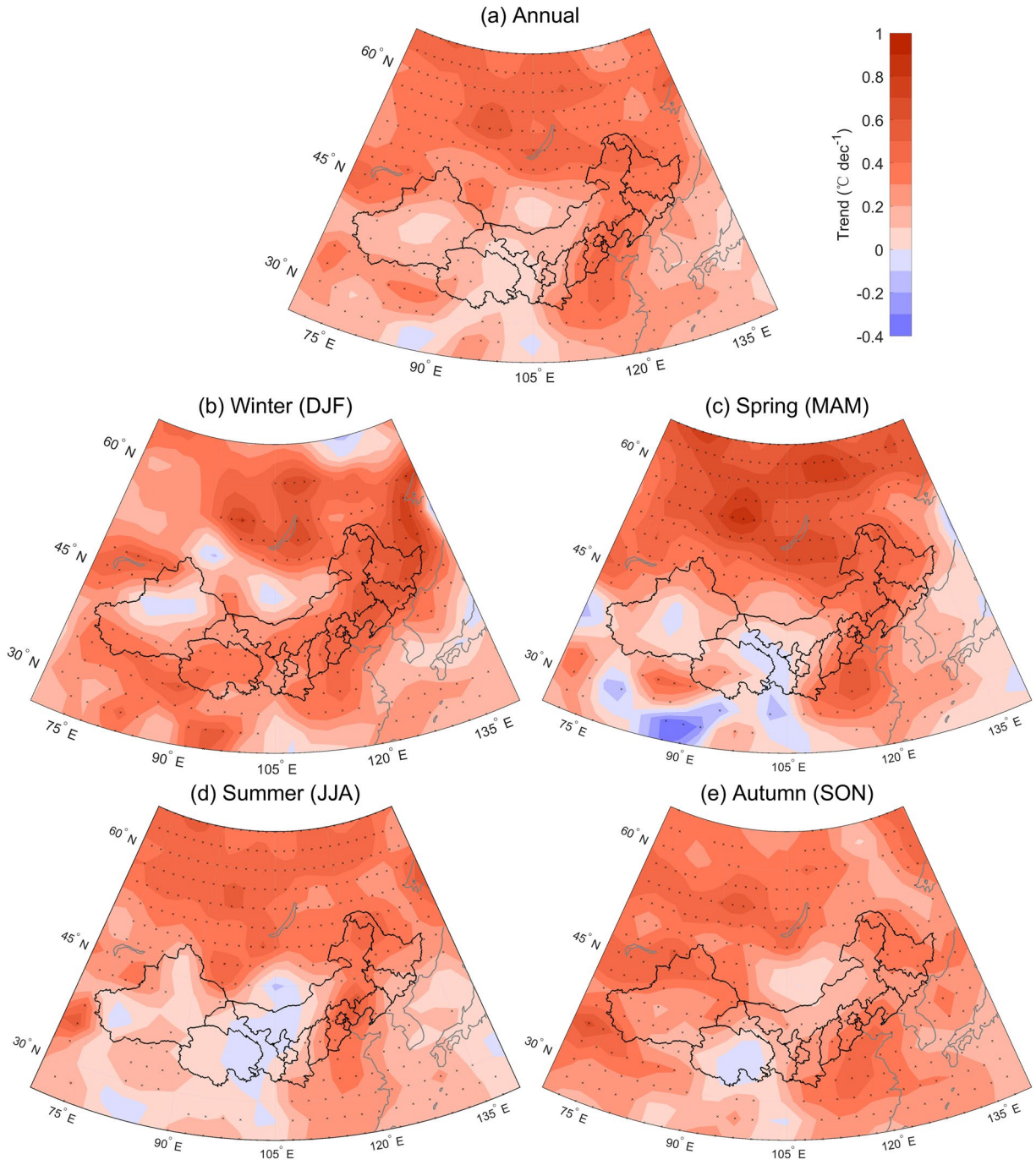

Figure 4. Spatial distribution of the sign and magnitude of annual and seasonal near-surface air temperature trends (in °C dec^{-1}) from the NCEP-NCAR1 reanalysis outputs over northern China and associated high-latitudes for 1961–2016. The black dots represent grid-cells having statistical significant trends at $p < 0.05$. The legend for part (a) applies to all other parts.

$p > 0.05$) was found for the southwest of northern China zone. A negative trend, but was not statistically significant (−0.14°C dec^{-1}, $p > 0.10$), was found in the near-surface air temperature gradient. Autumn near-surface wind speed anomalies correlated significantly with the near-surface air temperature gradient ($r = 0.25$, $p < 0.05$, Table 3). Moreover, the significant ($p < 0.05$) positive correlation between wind speed from NCEP-NCAR1 and air temperature gradient for 1961–2016 was found in the annual and all seasons, except autumn (Table 3). When looking at the change of air temperature in ERA5, ERA-Interim and NCEP-NCAR2 from 1979 to 2016 (Figures 5, S5, S6, and S7), the uneven warming pattern cannot be clearly seen,

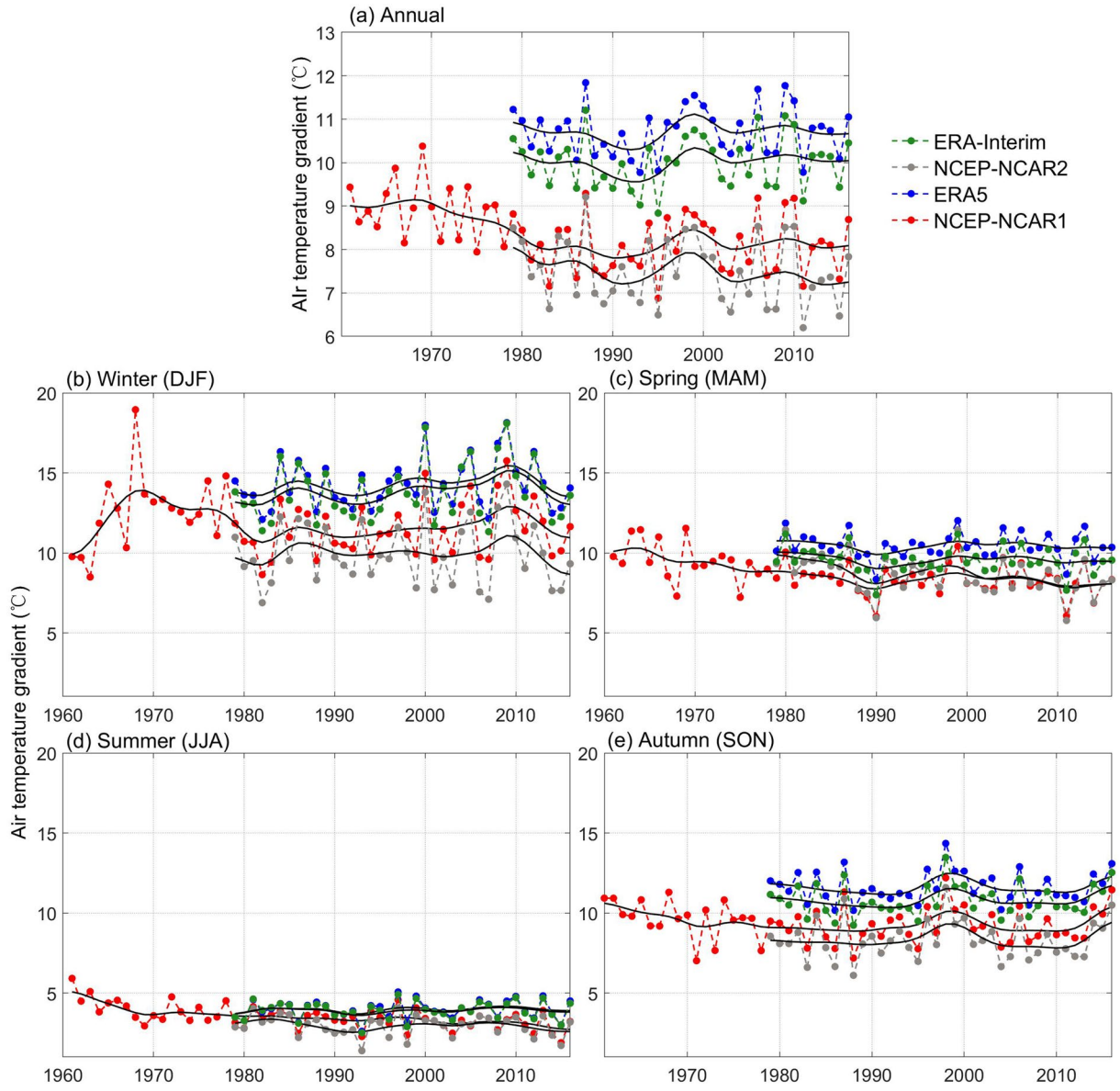

Figure 5. Annual and seasonal surface air temperature gradient between the high-latitude zone and the northern China zone from NCEP-NCAR1 reanalysis outputs for 1961–2016, and from ERA5, ERA-Interim and NCEP-NCAR2 reanalysis outputs for 1979–2016. The 11-year Gaussian low-pass filters are drawn in solid lines. The legend for part (a) applies to all other parts.

and trends of air temperature gradient were not significant ($p > 0.1$) (Table 3). The above results are in line with NCAR-NCAR 1 from 1979 to 2016 (Figure S8 and Table 3), and they resemble the multi-decadal variability as revealed by NCEP-NCAR1.

Figures 6 and 7 show the annual and seasonal spatial variability and temporal trends in the near-surface air pressure and in the air pressure gradient between the high-latitude zone and the northern China zone. Annual average air pressure increased significantly over most of the northern China zone (0.00 to +1.00 hPa dec^{-1}, $p < 0.05$) and decreased over most of the high-latitude zone (−0.20 to 0.00 hPa dec^{-1}, $p > 0.05$). This difference gives a significant negative trend in the air pressure gradient between the high-latitude zone and the northern China zone (−0.38 hPa dec^{-1}, $p < 0.05$) which correlates significantly with the weakening winds over northern China ($r = 0.57$, $p < 0.05$: Figures 6 and 7).

Table 3
Trend of Air Temperature Gradient (°C Decade^{-1}) and Pressure Gradient (hPa Decade^{-1}) From NCEP-NCAR1, ERA5, ERA-Interim, and NCEP-NCAR2, and Their Correlation With Wind Speed From Observation (Correlation Coefficient 1) and Reanalysis (Correlation Coefficient 2) Over Northern China

Time period			Air temperature gradient					Air pressure gradient				
			Annual	Winter	Spring	Summer	Autumn	Annual	Winter	Spring	Summer	Autumn
1961–2016	NCEP-NCAR1	Trend	−0.20	−0.12	−0.33	−0.24	−0.14	−0.34	−0.43	−0.38	−0.20	−0.29
		Correlation coefficient 1	**0.59**	**0.38**	**0.57**	**0.58**	**0.25**	**0.57**	**0.35**	**0.42**	**0.37**	**0.43**
		Correlation coefficient 2	**0.47**	**0.39**	**0.47**	**0.37**	−0.08	0.19	−0.07	0.08	**0.42**	−0.06
1979–2016	NCEP-NCAR1	Trend	0.00	0.24	−0.08	(-0.16)	0.10	0.00	0.25	(0.19)	−0.03	0.10
		Correlation coefficient 1	0.25	0.21	**0.37**	**0.49**	0.12	−0.02	0.07	0.03	−0.05	0.10
		Correlation coefficient 2	**0.50**	0.19	**0.42**	0.13	−0.19	0.13	0.02	**−0.29**	0.27	−0.10
	ERA5	Trend	0.00	0.13	0.00	0.02	0.02	−0.12	−0.06	**−0.29**	0.04	−0.06
		Correlation coefficient 1	0.25	0.20	**0.33**	0.25	0.15	(0.29)	0.16	**0.35**	−0.13	(0.32)
		Correlation coefficient 2	**0.48**	0.23	**0.44**	(0.29)	−0.04	**0.34**	0.25	0.09	−0.05	0.22
	ERA-Interim	Trend	0.02	0.23	−0.05	0.02	0.05	(-0.14)	−0.12	**−0.30**	0.05	−0.07
		Correlation coefficient 1	0.24	0.19	**0.36**	**0.31**	0.12	**0.33**	0.19	**0.37**	−0.13	**0.35**
		Correlation coefficient 2	**0.62**	**0.46**	**0.39**	**0.37**	**0.31**	0.17	0.04	0.02	−0.08	**0.36**
	NCEP-NCAR-2	Trend	0.00	0.13	0.00	0.02	0.02	−0.10	0.10	**−0.30**	−0.05	0.03
		Correlation coefficient 1	**0.44**	0.27	**0.52**	**0.48**	0.16	0.08	0.08	0.13	−0.04	0.18
		Correlation coefficient 2	**0.46**	0.25	**0.36**	−0.01	−0.19	0.10	0.12	−0.09	0.22	−0.23

Note: Statistically significant level defined as those $p < 0.10$ are in parenthesis and $p < 0.05$ are bolded.

The winter near-surface pressure gradient increased significantly over most of the northern China zone (0.00 to +0.60 hPa dec^{-1}, $p < 0.05$), while negative trends were found in the high-latitude zone, but were not significant (−0.50 to 0.00 hPa dec^{-1}, $p > 0.10$: Figures 6 and 7). The gradient in near-surface air pressure between the high-latitude zone and the northern China zone, therefore, declined significantly (−0.43 hPa dec^{-1}, $p < 0.05$). Note that Figure 7b shows a sudden increase in the winter near-surface pressure gradient around the 2000s, which is consistent with the recovery of winter near-surface wind speeds seen in recent decades, see Figure 2b. Moreover, there was an absolute low value of air pressure gradient in 2007, which is due to interannual variability of atmospheric circulation with a similarly low value of winter air temperature gradient and wind speed found in 2007. This suggests that interannual variability of wind speed is also related to winter air pressure variation. The correlation between the near-surface pressure gradient and near-surface wind speeds is significant ($r = 0.35$, $p < 0.05$). A similar spatial pattern was found for near-surface pressure changes in spring, creating a negative trend in the surface pressure gradient (−0.38, $p < 0.05$), which correlates significantly with near-surface wind speed ($r = 0.42$, $p < 0.05$). Near-surface air pressure increased significantly in summer and autumn in the northern China zone (+0.20 to +1.00 hPa dec^{-1}, $p < 0.05$), while it decreased in the high-latitude zone. The positive trends were significant for summer air pressure in the middle and eastern parts of our study region (0.0 to +0.6 hPa dec^{-1}, $p < 0.05$), while the autumn trend in the western part of the region was negative but not significant (−0.20 to 0.0 hPa dec^{-1}, $p > 0.05$) and was slightly positive in eastern parts of the region. These differences result in a significant decline in the near-surface air pressure gradient for spring and autumn (−0.20 and −0.29 hPa dec^{-1}, $p < 0.05$, respectively), which is associated with reduced near-surface wind speeds (the correlation between the near-surface pressure gradient and near-surface wind speed corresponds to $r = 0.37$ and 0.43 for spring and autumn, respectively: Figures 6 and 7). Furthermore, the relation between near-surface wind speed from NCEP-NCAR1 and air pressure gradient for 1961–2016 was also examined (Table. 3), and a significant ($p < 0.05$) correlation was only detected in summer. The similar spatial pattern of air pressure changes from ERA5, ERA-Interim and NCEP-NCAR1 (Figures S9, S10, and S11) was found in annual and all seasons, except winter, for 1979–2016, resulting in the declined pressure gradient between the high-latitude zone and the northern China zone (Figure 7 and Table. 3). The above results concur with NCAR-NCAR 1 from 1979 to 2016 (Figure S12 and

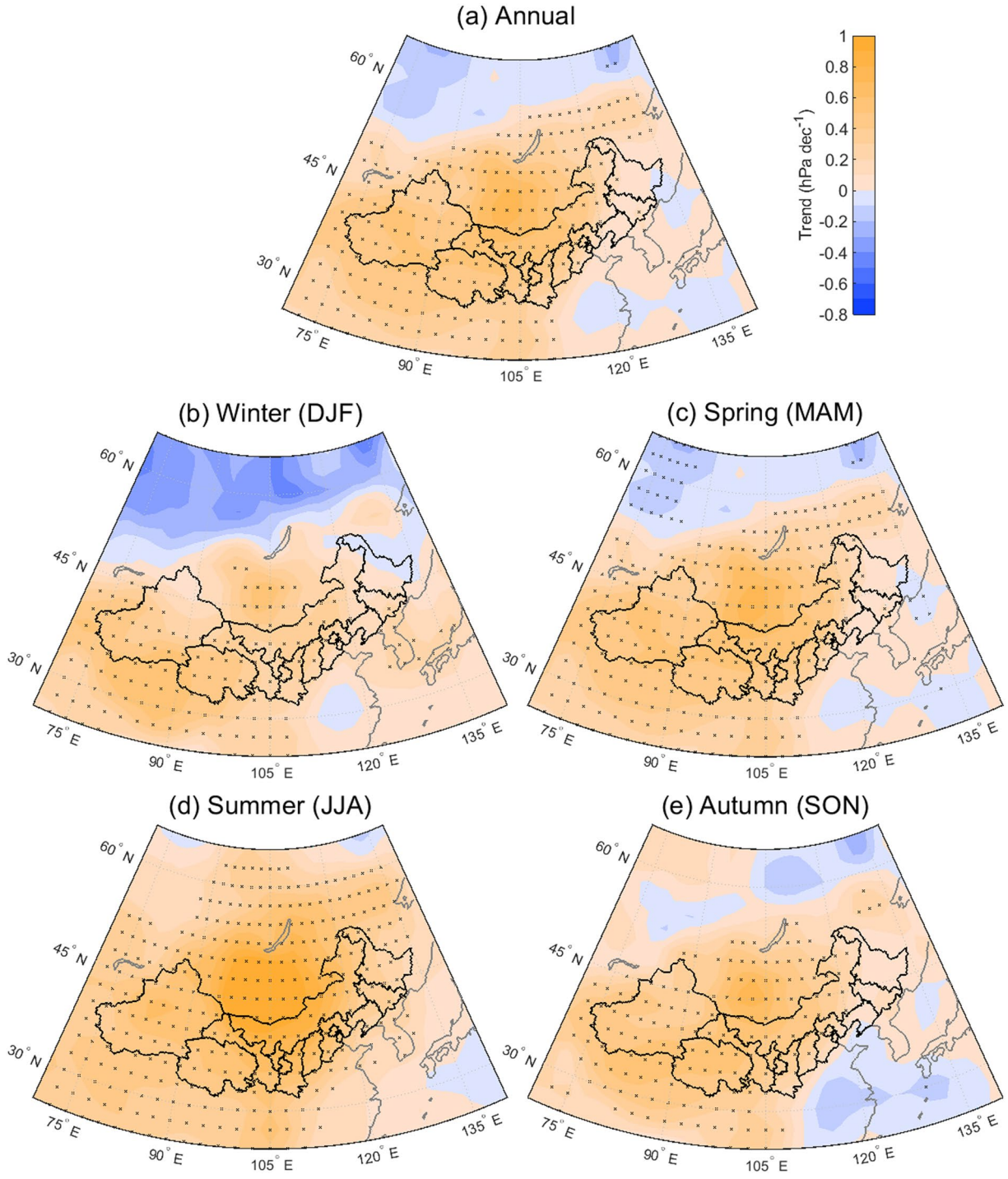

Figure 6. Spatial distribution of sign and magnitude of annual and seasonal surface air pressure trends (hPa dec^{-1}) from the NCEP-NCAR1 reanalysis outputs over northern China and associated high-latitudes for 1961–2016. Black dots represent grid-cells having statistically significant trends at $p < 0.05$. The legend for part (a) applies to all other parts.

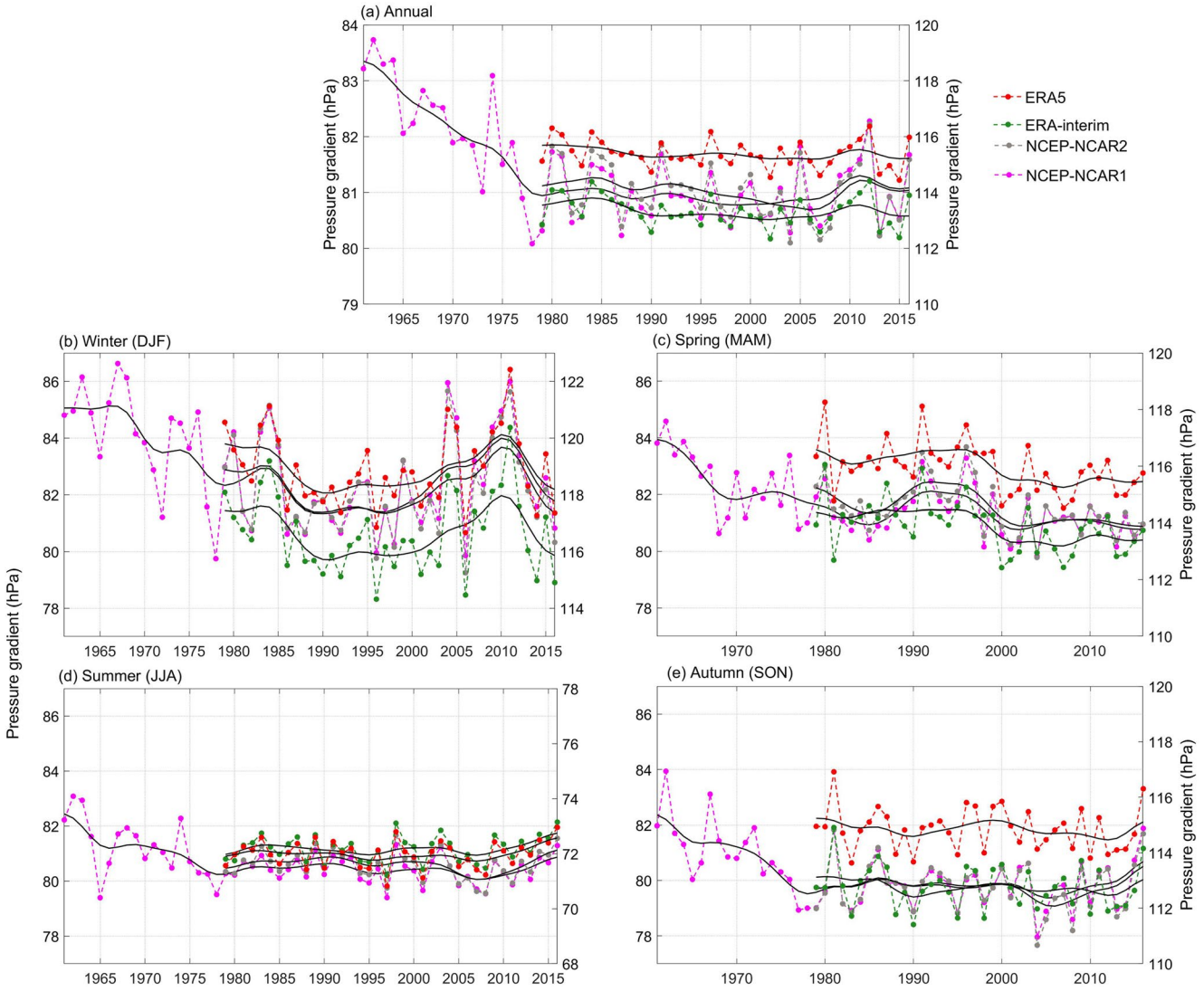

Figure 7. Annual and seasonal surface air pressure gradient between the northern China zone and the high-latitude zone from the NCEP-NCAR1 reanalysis outputs for 1961–2016 and from ERA5, ERA-Interim and NCEP-NCAR2 reanalysis outputs for 1979–2016. Note a right *Y*-axis label is for ERA5 and ERA-Interim. The 11-year Gaussian low-pass filters are drawn in black solid lines. The legend for part (a) applies to all other parts.

Table 3), and they generally resembled the same multi-decadal variability of air pressure gradient as the NCEP-NCAR1 results (Figure 7).

3.3. Changes to Surface Air Temperature in CAM5-All and CAM5- Nat

Figure 8 shows trends in the annual and seasonal surface air temperature in the CAM5-All and CAM5-Nat simulations for 1961–2016. Changes in the air temperature gradient between the high-latitude zone and the northern China zone from the CAM5-All and CAM5- Nat simulations are shown in Figure 9. Annual air temperatures in CAM5-All increased significantly in the high-latitude zone (0.20°C dec^{-1} to 0.70°C dec^{-1}, $p < 0.05$), and increased more slightly in northern China zone (0.00°C dec^{-1} to 0.30°C dec^{-1}, $p < 0.05$, Figure 8a). This difference results in a significantly weakened air temperature gradient (−0.14°C dec^{-1}, $p < 0.05$) between the high-latitude zone and northern China zone (Figure 9a). In the CAM5-Nat simulations, air temperature trends were not significant in the high-latitude zone or in the northern China zone (−0.2°C dec^{-1} to 0°C dec^{-1}, $p > 0.05$, Figure 8b), resulting in a stable air temperature gradient between the two zones (−0.02°C dec^{-1}, $p > 0.10$, Figure 9b).

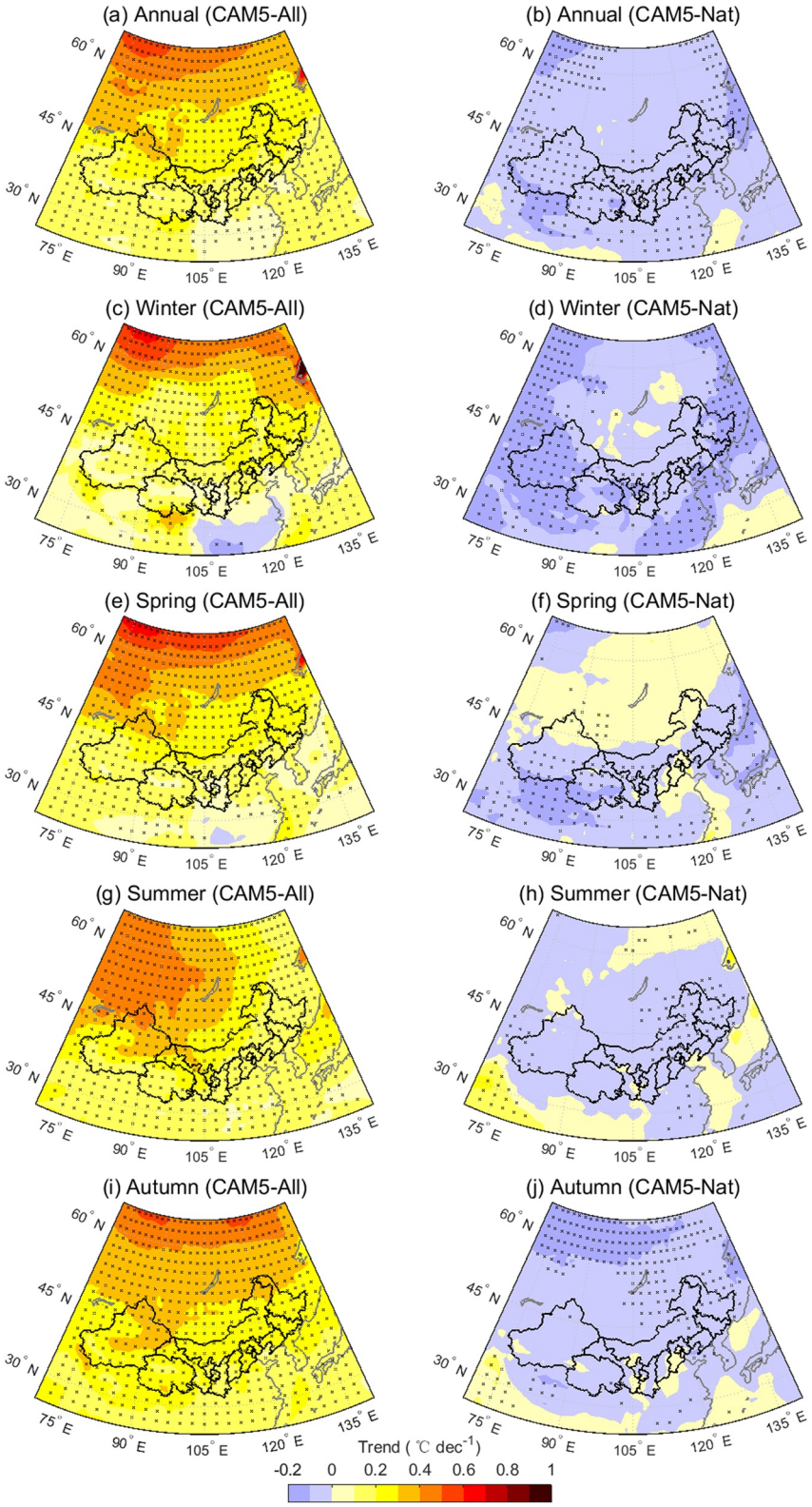

Figure 8. Spatial distribution of sign and magnitude of near-surface air temperature trends (°C dec^{-1}) in CAM5-All (left column) and CAM5-Nat (right column) over the northern China zone and the associated high-latitudes zone for 1961–2016. The black dots represent grid-cells having statistically significant trends at $p < 0.05$.

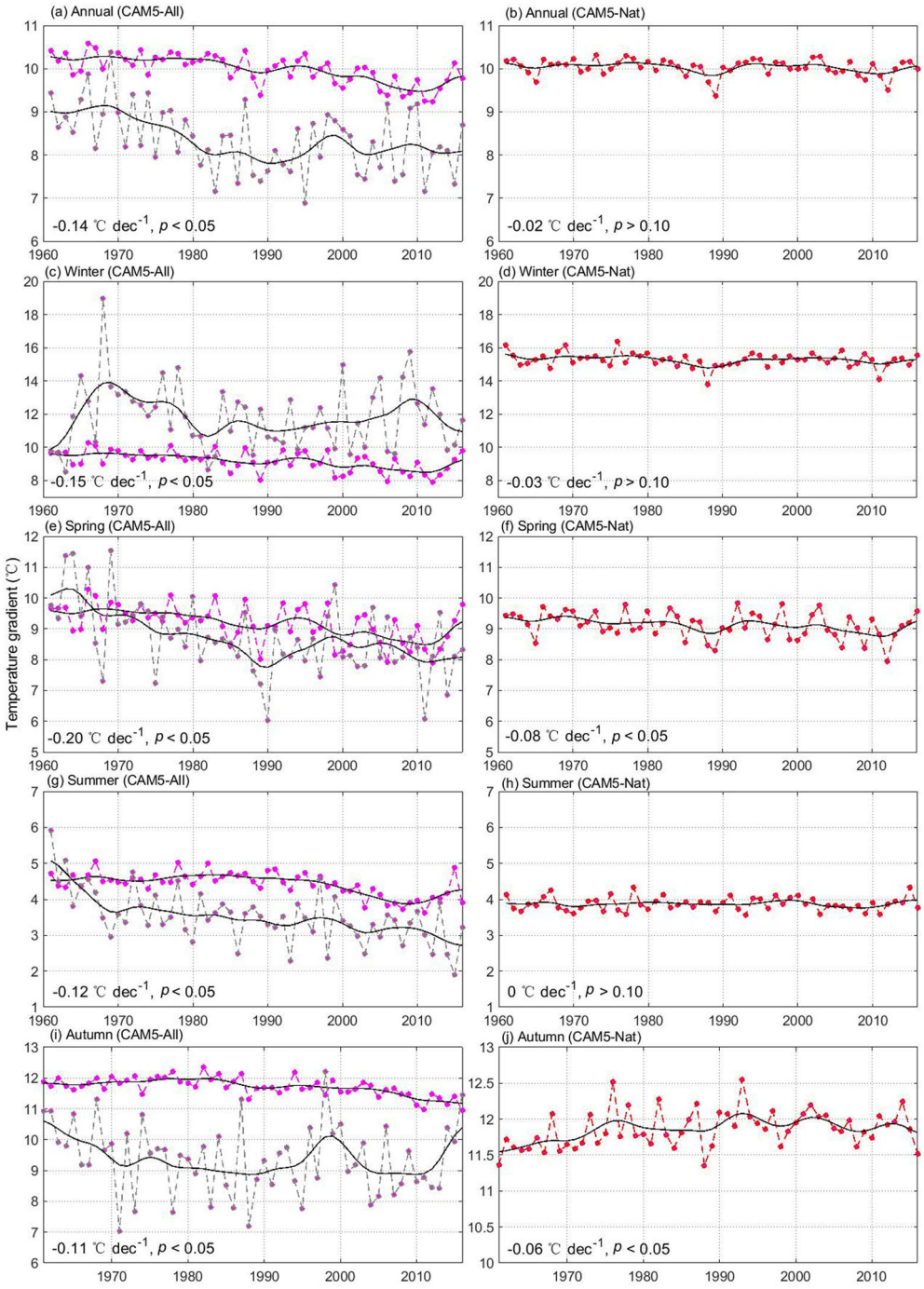

Figure 9. Simulated annual and seasonal near-surface air temperature gradients (°C) from CAM5-All (left column) and CAM5-Nat (right column) between the high-latitude zone and the northern China zone for 1961–2016. Note that air temperature gradient (°C) from NCEP-NCAR1 (in gray) is displayed in the left column. The black solid lines indicate the 11-year Gaussian low-pass filter. Magnitude (°C dec^{-1}) and significant level of trends are displayed in each plot. To enable comparisons between the "All" and "Nat" CAM5 models, the ordinates (i.e., *Y*-axes) have the same extents and intervals for each pair of plots.

Winter air temperatures increased rapidly in the high-latitude zone (0.10°C dec^{-1} to 0.80°C dec^{-1}, $p < 0.05$) and increased slightly in the northern China zone (0.00°C dec^{-1} to 0.30°C dec^{-1}, $p < 0.05$) in the CAM5-All simulations (Figure 8c). This uneven warming pattern results in a significant decline in the near-surface air temperature gradient (−0.15°C dec^{-1}, $p < 0.05$, Figure 9c) between the two zones. In the CAM5- Nat

simulations, slight decreases were found over most of the high-latitude zone and the northern China zone, but these were not significant (−0.2°C dec^{-1} to 0°C dec^{-1}, $p > 0.05$, see Figure 8d), and no significant change in the near-surface pressure gradient was detected (−0.03°C dec^{-1}, $p > 0.1$, Figure 9d). Note that the air temperature gradient in CAM5-Nat simulations was higher than in CAM5-All simulation, this might be due to the warm bias in the CAM model (Xu & Yang, 2015). There were significant warming trends in the high-latitude zone for spring in the CAM5-All simulations (0.2°C dec^{-1} to 0.8°C dec^{-1}, $p < 0.05$) and weaker warming trends in the northern China zone (0–0.3°C dec^{-1}, $p < 0.05$, Figure 8e), creating a significant decrease in the near-surface air temperature gradient (−0.20°C dec^{-1}, $p < 0.05$, Figure 9e). In the CAM5-Nat simulations, near-surface air temperatures showed slight warming trends over most of the high-latitude zone and weak cooling trends in the northern China zone (Figure 8f), corresponding to a slightly decreased near-surface air temperature gradient between the two zones (−0.08°C dec^{-1}, $p < 0.05$, Figure 9f). The summer near-surface air temperature gradient also increased significantly in the CAM5-All simulations (−0.12°C dec^{-1}, $p < 0.05$, Figure 9g), as a result of rapid warming trends in the high-latitude zone (0°C dec^{-1} to 0.8°C dec^{-1}, $p < 0.05$) and weaker warming trends in the northern China zone (0°C dec^{-1} to 0.4°C dec^{-1}, $p < 0.05$, Figure 8g). However, in the CAM5-Nat simulations, changes in near-surface air temperature were small in both zones (−0.1°C dec^{-1} to 0.1°C dec^{-1}, $p > 0.05$, see Figure 8h), and there was no trend in the near-surface temperature gradient (0°C dec^{-1}, $p > 0.1$, see Figure 9h) between the two zones. The spatial pattern in near-surface air temperature changes in autumn was similar to the one found for summer. That is, uneven distribution of the warming in the CAM5-All simulations resulted in a negative near-surface air temperature trend (−0.11°C dec^{-1}, $p < 0.05$, see Figure 8i), while in the CAM5-Nat simulations, most of the high-latitude zone and the northern China zone corresponded to a slight cooling trend (−0.1 to 0, $p > 0.05$, see Figure 8j). The near-surface air temperature gradient trend in the CAM5-Nat simulations was, therefore, weaker than that in the CAM5-All simulations (−0.06°C dec^{-1}, $p < 0.05$, see Figure 9j).

3.4. Changes to Near-Surface Wind Speed in the CAM5-All and CAM5-Nat Simulations

Figure 10 shows trends in the simulated annual and seasonal near-surface wind speed anomalies (calculated relative to the 1981 to 2010 mean), and the variability in these anomalies for CAM5-All and CAM5-Nat over northern China for 1961 to 2016. The spatial distribution of the annual and seasonal near-surface wind speed trends is shown in Figure 11. A statistically significant decline in mean annual near-surface wind speed was found for the CAM5-All simulations (−0.008 m s^{-1} dec^{-1}, $p < 0.05$), with the most rapid decrease occurring between 1970 and 1990, see Figure 10a, after which near-surface wind speeds became stable. Annual near-surface wind speed was significantly correlated with the simulated air temperature gradient from CAM-All ($r = 0.72$, $p < 0.05$). Moreover, significant negative near-surface wind speed trends in northern China, particularly in the western part of the study region (Figure 11a), agree with the observed near-surface wind speed trends in Figures 2a and 3a. In the CAM5-Nat simulations, a weaker significant negative trend in near-surface wind speed was simulated (−0.005 m s^{-1} dec^{-1}, $p < 0.05$, Figure 10b), while trends simulated over most of northern China were not significant ($p > 0.05$, Figure 11b).

The CAM5-All simulations of winter near-surface wind speed show a significant negative trend (−0.009 m s^{-1} dec^{-1}, $p > 0.1$, Figure 10c) having a significant correlation with the air temperature gradient ($r = 0.59$, $p < 0.05$). The rapid decline from 1970 to 1990 and stabilization after 1990 concur with patterns in the observed near-surface wind speed (Figure 2b). Negative near-surface wind speed trends were calculated for most of northern China, particularly in the western and middle parts (Figures 11c). In CAM5-Nat, near-surface wind speeds fluctuated strongly over the 56-years, although there was a negative trend, it was not significant (−0.002 m s^{-1}dec^{-1}, $p > 0.0$, Figure 10d). Most of northern China corresponded to an insignificant negative near-surface wind speed trend in the CAM5-Nat simulations (Figures 11d). Spring near-surface wind speeds declined significantly in the CAM5-All simulations (−0.009 m s^{-1} dec^{-1}, $p < 0.05$, Figure 10e), with most areas experiencing negative trends (Figures 11e). This pattern agrees with the observed near-surface wind speed data (Figure 3c). A significant correlation between wind speed and air temperature gradient in the CAM-All simulations was found. Note that a steadily weakening near-surface wind speed was calculated in CAM5-Nat (−0.008 m s^{-1} dec^{-1}, $p < 0.05$, Figure 10f), while most of northern China experienced insignificant ($p > 0.05$) negative near-surface wind speed trends (Figures 11f). There was a weak negative trend in the summer near-surface wind speed calculated in CAM5-All (−0.004 m s^{-1} dec^{-1}, $p > 0.1$, Figure 10g), with a weak correlation ($r = -0.08$, $p > 0.1$) between near-surface wind speed and air

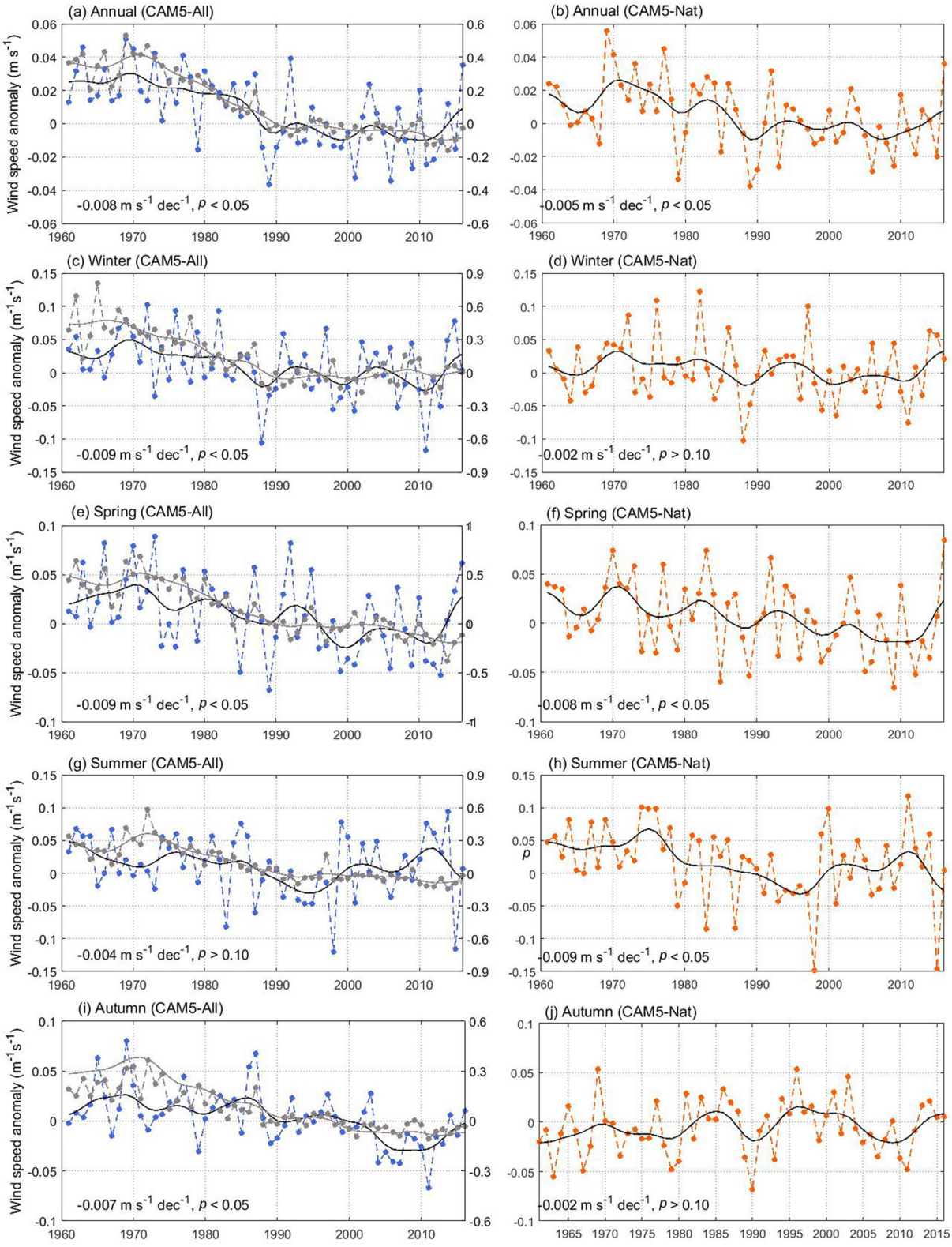

Figure 10. Simulated annual and seasonal mean wind speed (m s^{-1}) in CAM5-All (left column) and CAM5-Nat (right column) over northern China for 1961–2016. Note that observed wind speed variability (m s^{-1}, the gray dots and line) is displayed in the left column with right *Y*-axis. The black solid lines indicate the 11-year Gaussian low-pass filter, magnitude (m s^{-1} dec^{-1}) and significant level of trends are displayed for each plot. To enable comparisons between the "All" and "Nat" CAM5 models, the ordinates (i.e., *Y*-axes) have the same extents and intervals for each pair of plots.

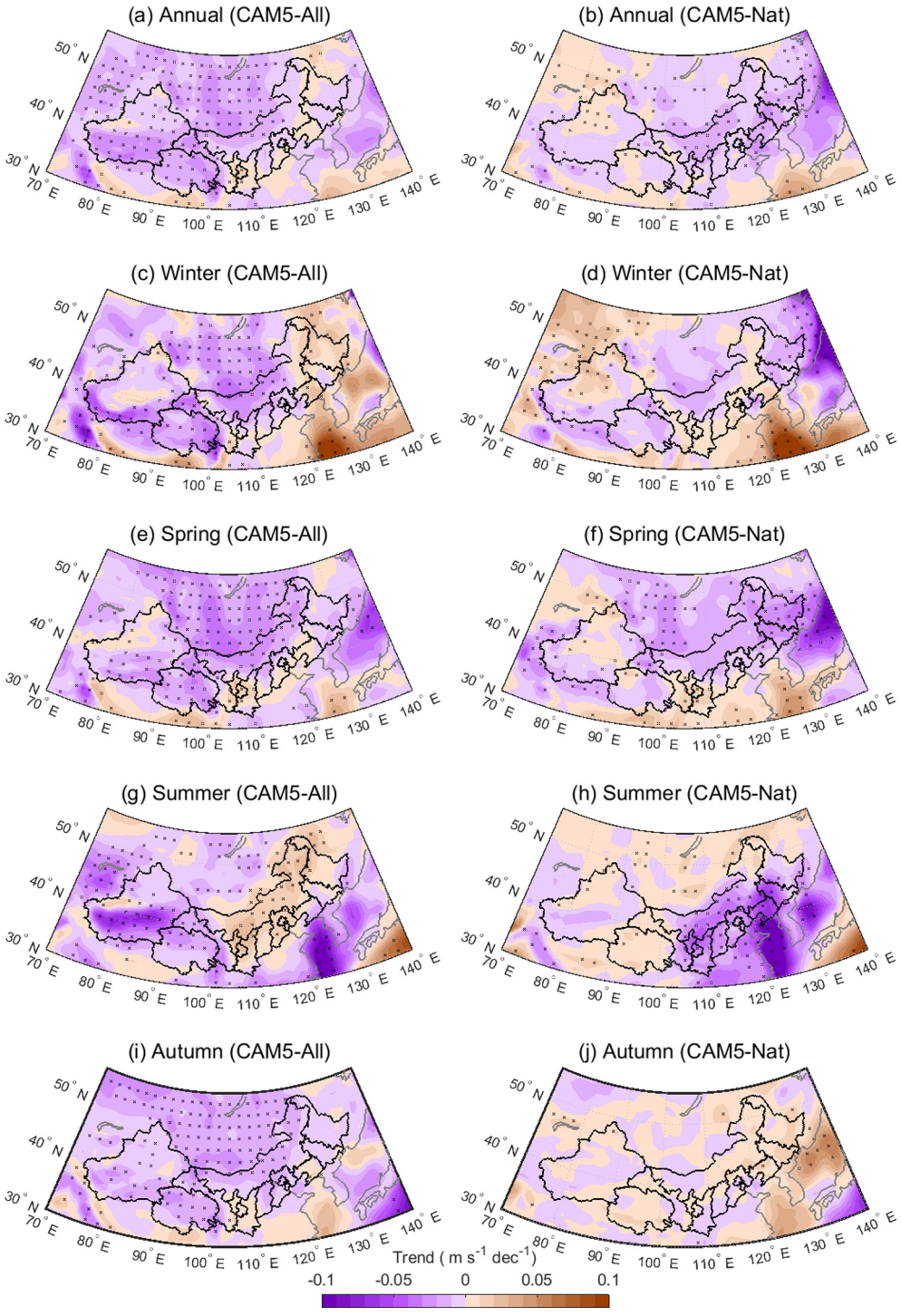

Figure 11. Spatial distribution of sign and magnitude of surface wind speed trends in CAM5-All and CAM5-Nat ($m\ s^{-1}\ dec^{-1}$) over northern China for 1961–2016. The black "x" symbols represent grid-cells having statistical significance at $p < 0.05$.

temperature gradient in CAM5-All simulations. There were significant ($p < 0.05$) negative trends in the western part of the region contrasting the significant ($p < 0.05$) positive trends in the eastern part of the study site (Figure 11g). This contrasts with the CAM5-Nat simulations, where significant negative near-surface wind speed trends with a greater magnitude were found ($-0.009\ m\ s^{-1}\ dec^{-1}$, $p < 0.05$, Figure 10h),

with significant ($p < 0.05$) negative trends in the eastern part of the study site (Figure 11h). CAM5-All simulations of autumn near-surface wind speed displayed significant negative trends (-0.007 m s^{-1} dec^{-1}, $p < 0.05$ (Figure 10i), and a significant stilling trend was simulated over most of northern China (Figure 11i). Near-surface wind speed was significantly related to the air temperature gradient in CAM5-All simulations. No significant ($p > 0.10$) near-surface wind speed trend (-0.002 m s^{-1} dec^{-1}) was simulated in CAM5-Nat (Figure 10j), and trends over the whole study area were insignificant at $p > 0.05$ (Figures 11j).

4. Discussion

We investigated the trends and the variabilities for homogenized mean near-surface wind speed data over northern China for 1961 to 2016, and found a significant negative trend in annual near-surface wind speed (-0.103 m s^{-1} dec^{-1}, $p < 0.05$), which agrees with the slowdown detected for some sub-regions in northern China (e.g., Y. Li et al., 2018; G. Zhang et al., 2019). This also concurs with the previously mentioned wind stilling that has been observed globally at mid-latitudes (McVicar et al., 2012). Note that most of stations are located in the central and east parts of northern China and a lack of stations occurs in some areas, for example, Tibet Plateau and Tarim Basin. However, wind speed variability is not overly sensitive to the number of stations (Figure S2). According to Azorin-Molina et al. (2014), wind series with few stations (Portugal, 8 stations in the western Iberian Peninsula; i.e., a different region), showed the same trends and multidecadal variability as wind series with a large data set (59 stations across Spain; central and eastern Iberian Peninsula). Multi-decadal near-surface wind speed variability over our study period fell into three phases: (i) strongly fluctuating near-surface wind speeds in the 1960s; (ii) rapidly declining near-surface wind speeds in the 1970 and 1980s; and (iii) relatively stable near-surface wind speeds from 1991 onwards, which agrees with previous investigations of all-China wind variability (Lin et al., 2013; G. Zhang et al., 2019). Recent wind studies (Azorin-Molina et al. 2019; Dunn et al. 2016; Zeng et al., 2019) reported a similar stabilization, or possibly a rebound, of global near-surface wind speeds that began the 2010s, following 30–50 years of decline. These findings suggest that the decline in near-surface wind speed halted around 20 years earlier in northern China (i.e., in 1991 rather than in the 2010s); consistent with the findings of Zeng et al. (2019). Most interestingly, we found distinct differences in near-surface wind speed evolution among seasons. For example, winter wind speed increased after 1990s, while near-surface wind speeds in other seasons were stable and even declined slightly since then. Recent studies (Azorin-Molina et al., 2019; Zeng et al., 2019) have shown that the sign and magnitude of near-surface wind speed trends show seasonal differences. We also assessed the variability of near-surface wind speed from NCEP-NCAR1 and found that magnitude of wind speed trends is much lower than observed wind speed, in line with others who reported that NCEP-NCAR1 failed to reproduce the stilling phenomenon in China (e.g., Chen et al., 2013) and elsewhere (e.g., Australia, McVicar et al., 2008 and USA, Pryor et al., 2009). While significant correlation between wind speed from the station observation and NCEP-NCAR1 was found ($r = 0.49$, $p < 0.05$ for seasonally averaged quantities), and multi-decadal variability of wind speed from NCEP-NCAR1 agreed with near-surface wind speed observations. Our results show that near-surface wind speed from NCEP-NCAR1 can only partly reproduce the wind speed variability from station-based observation.

The high-latitudes of Eurasia experienced faster warming than middle- and low-latitudes over recent decades (IPCC, 2013), resulting in an uneven warming pattern and a weakening of the air temperature gradient between high- and middle/low-latitudes (Y. Li et al., 2018; You et al., 2014), as the high-latitude zone displayed a lower near-surface air temperature and higher near-surface air pressure (see Figure S13).We also investigated air temperature gradient from gridded in situ observations (Figure S14), and found significant correlation ($r = 0.87$, $p < 0.05$, for seasonally averaged quantities) between in situ observations and NCEP-NCAR1, with a strong consistency with NCEP-NCAR1, that is, rapidly declined trends from 1970 to 1990s and recovered trends since 2000s. We also detected that air temperature gradient is higher from in situ observations than from NCEP-NCAR1, which might be associated with the nonuniform stations distribution and/or be an inherent limitation of NCEP-NCAR1; unraveling this is a topic for further research. This uneven warming also modulates the pressure gradient through thermodynamic adaption (Lin et al., 2013), and so influences wind dynamics. Here, we found a substantial decline in annual and seasonal air temperature gradient between a high-latitude zone and the northern China zone, and showed significant positive correlations between this gradient and near-surface wind speed ($r = 0.59$, $p < 0.05$, for seasonally averaged

quantities). The rapid decline in the air temperature gradient and air pressure gradient in the 1970 and 1980s between these two zones, and the stabilization or slight recovery that we found to have occurred from the 1990s onwards, is consistent with observed multi-decadal near-surface wind speed variability across north China. Moreover, we found that air temperature and large-scale pressure gradients between these two zones together can partly explain the variance of wind speed variability (47.66%, $p < 0.05$, for seasonally averaged quantities, see Table S1). This suggests that other factors such as regional-local scale pressure gradients also play a key role in modulating near-surface wind speed (Belušić Vozila et al., 2019). The substantial decrease in the annual and seasonal air pressure gradient concurs with weakened Siberian and Mongolian high pressure anomalies (R. Zhang et al., 2019) and is significantly correlated with near-surface wind speed anomalies (e.g., $r = 0.57$, $p < 0.05$ for seasonally averaged quantities). For example, Chen et al. (2013) showed that a Northern Hemisphere large-scale teleconnection index, that is, the AO, is significantly correlated with near-surface wind speeds across China. They also found that positive AO is linked to a weakened Siberian High, leading to a large-scale pressure gradient decline and thus a reduction in near-surface wind speeds. Our study has further investigated how uneven warming-induced meridional air pressure gradient reduction, causing declined near-surface wind speed in northern China. Note that climate signals shown in our results do not follow the boundary of northern China study site, which means that uneven warming might have an impact on wind speed changes across other neighboring regions (e.g., central China). However, previous studies highlighted that wind speed over central and southeast China is primarily modulated by the land-sea pressure gradient (e.g., East Asian summer monsoon, Xu et al., 2006; Zhu et al., 2012). Therefore, wind speed changes over central China are more complex, which could be jointly affected by meridional (i.e., latitudinal) temperature gradient and the land-sea pressure gradient (Xu et al., 2006; R. Zhang et al., 2019). We selected northern China as our study region, not including central China, as near-surface wind speed in northern China is mainly driven by one factor (i.e., westerly and East Asian winter monsoon as a result of large-scale meridional gradient changes, Y. Li et al., 2018) making it more amenable to unraveling the association with warming when compared to central China. More comprehensive analyses are strongly needed to reveal the physical processes behind near-surface wind speed changes across other regions like central and southeast China; which is beyond the scope of this research. Additionally, it can be interesting for future studies to examine how uneven warming has affected tropospheric wind speed changes, as near-surface wind speed is modulated by tropospheric atmospheric circulation change through thermal and dynamic momentum downward transport (Zhang et al., 2020).

In this study, we provided the first evidence of the contribution of uneven warming to changes in near-surface wind speed based on the CAM5 historical climate model simulations, driven by "all forcing" including anthropogenic emissions or driven only by "natural forcing". The uneven warming pattern simulated in CAM5-All results in a significant ($p < 0.05$) declining air temperature gradient (-0.14°C dec^{-1}, for seasonally averaged quantities) and significant ($p < 0.1$) declining air pressure gradient (-0.01 hPa dec^{-1}, for seasonally averaged quantities, Figures S15 and S16), while trends in air temperature were insignificant in CAM5-Nat and trends in air pressure increased in the high-latitude zone and declined in the northern China zone (Figure S15). As a result, the air temperature gradient remained practically unchanged (-0.02 hPa dec^{-1}, $p > 0.1$, for seasonally averaged quantities), whereas there was a significantly increased air pressure gradient in CAM5-Nat ($+0.06$ hPa dec^{-1}, $p < 0.05$, for seasonally averaged, Figure S16). Note that warming biases can exist in CAM model simulation, like RegCM (Güttler, 2011). But since we are concerned with gradient here, the effect of bias should be to a large extent removed. The observed widespread decline in near-surface wind speed was realistically represented in CAM5-All in both the annually and seasonally averaged data, except for summer, where CAM5-All simulated near-surface wind speed trends were one order of magnitude smaller than those observed. CAM5-Nat simulated widespread insignificant trends in annually and seasonally averaged near-surface wind speeds, except summer. This demonstrates that stilling in northern China was at least partly driven by uneven warming. Near-surface wind speeds simulated in CAM5-All displayed the three distinct phases mentioned previously, while there were no obvious phases in the CAM5-Nat simulated near-surface wind speeds. The phases seen in the CAM5-All simulated near-surface wind speeds are consistent with observed near-surface wind speed changes and air temperature gradient variability, which confirms that multi-decadal changes in near-surface wind speeds over northern China are at least partially driven by the air temperature gradient, and shows that the recovery or stabilization of near-surface wind speeds was most likely driven by the stabilization of the temperature gradient. It should

be noted that negative near-surface wind speed trends were underestimated in the CAM5-All simulations, relative to observations, which implies a large systematic bias in long-term climate model simulations. This bias is noted in Chen et al. (2012), who reported that CMIP-5 historical simulations were unable to realistically capture the stilling phenomenon. Given increased friction is another well-established factor for wind stilling (e.g., Vautard et al., 2010; Wever, 2012; Z. Zhang et al., 2019) and it is held constant in most models including the one used herein, the underestimated decreasing trend by model simulations might be related to surface roughness changes. Therefore, improving the ability of climate models in simulating wind changes is urgently needed. The observed slow-down of global warming during the last two decades (Kosaka & Xie, 2013; Wohland et al., 2019), known as the "warming hiatus" has resulted in an increase in the temperature gradient between high- and middle/low-latitudes. This may be a driver for the recent recovery of terrestrial near-surface wind speeds that has been widely reported across the globe (Azorin-Molina et al., 2018; Kim & Paik, 2015; Zeng et al., 2019).

Here, we confirmed that uneven warming has partly contributed to the declined trend in annual and seasonal near-surface wind speeds over northern China. Declining near-surface wind speed trends were simulated in CAM5-Nat for annual averages and for some seasons, which indicates that the natural variability also plays a role in regulating the variation of near-surface wind speed in northern China. This is confirmed by a periodic change in wind activity over northern China from ~1850 to ~1950 (Xu et al., 2019), that is, over a period with relatively low anthropogenic emissions of greenhouse gases and aerosols compared to 1960–2016. Note that differences in wind speed evolution among seasons were not fully related to the differences of the air temperature and pressure gradients, which means that other physical processes also affected wind speed. For instance, wind speed in northern China was partly regulated by synoptic circulation systems (i.e., extratropical cyclones, Zhang et al., 2020). Increased surface roughness resulting from forest growth and urbanization is another cause for global terrestrial wind stilling (Z. Li et al., 2018; Vautard et al., 2010; Z. Zhang et al., 2019). Vegetation greening has been observed in northern China partly in response to ecological conservation policies implemented by the Chinese government over recent decades (Piao et al., 2015; Zhu et al., 2016). These, along with the rapidly growing Chinese economy and the associated urbanization of northern China (Bai et al., 2014), could partly explain the decline in near-surface wind speeds from 1970 to 1990. However, the reversal in terrestrial near-surface wind speed trends that has been observed since 1990 is not consistent with continuing increased surface roughness. This implies that decadal variations in near-surface wind speed in northern China are likely to be primarily driven by changes in atmospheric circulation. Nevertheless, the consistently increasing surface roughness over recent years (2000–2018) is likely to be postponing or attenuating the observed recovery or stabilization of near-surface wind speeds. To fully understand the drivers of regional near-surface wind speed dynamics, the research community must better quantify the contribution of each driver of near-surface wind speed changes through conducting "sensitivity analysis" experiments in state-of-the-art climate models. Such models are a valuable tool to explore those kinds of questions, and high-resolution products of the CORDEX group should be used (Moemken et al., 2018) to study the multi-decadal near-surface wind speed variability.

5. Conclusion

Referring to our stated aim and three specific objectives, our main findings are summarized as follows.

1. Overall, near-surface wind speed has declined over northern China based on the homogenized near-surface wind speed data assessed here. Annual mean near-surface wind speed showed a significant declining trend (-0.103 m s^{-1} dec^{-1}, $p < 0.05$), and seasonal trends showed a similar pattern, with the highest negative trend for spring (-0.137 m s^{-1} dec^{-1}), and the lowest negative trend for summer (-0.078 m s^{-1} dec^{-1}). Annual mean and seasonal near-surface wind speeds were found to have stabilized from 1990 onwards.
2. Rapid warming at high-latitudes has weakened the air temperature gradient (-0.32°C dec^{-1} to 0.12°C dec^{-1}) between the high-latitude zone and the northern China zone from 1961 to 2016, and this has driven a decline in the air pressure gradient between the two zones (-0.42 to -0.20 hPa dec^{-1}), which is likely to have contributed to the decline in observed near-surface wind speed over the study site. Multi-decadal variations in annual and seasonal near-surface wind speeds were consistent with variations in the air temperature gradient, and the two were shown to be significantly correlated ($p < 0.05$).

3. Historical climate model simulations showed that the uneven warming was captured realistically in the CAM5-All simulations, both annually and seasonally. While CAM5-Nat simulations displayed only insignificant ($p > 0.1$) changes in the annual and seasonal air temperature gradient between the high-latitude zone and the northern China zone, suggesting that the uneven warming pattern was driven by anthropogenic emissions.
4. Widespread significant ($p < 0.05$) negative near-surface wind speed trends were found over northern China in the CAM5-All simulations, except for summer; meanwhile in the CAM5-Nat simulations, not significant ($p > 0.05$) changes to near-surface wind speed occurred, except for summer. This confirms that the decline in near-surface wind speed observed over northern China is at least partly attributable to the uneven warming pattern.

Data Availability Statement

Wind speed from station observations can be accessed at China Meteorological Administration (CMA; http://data.cma.cn/en), observed air temperature data were downloaded from the Global Historical Climatology Network (https://www.ncdc.noaa.gov/data-access/land-based-station-data/land-based-datasets/global-historical-climatology-network-ghcn), NCEP–NCAR1 Reanalysis were retrieved from NOAA (https://www.esrl.noaa.gov/psd/data/gridded/data.ncep.reanalysis.pressure.html), ERA5 Reanalysis and ERA-Interim Reanalysis were downloaded from ECMWF (https://cds.climate.copernicus.eu/), NCEP-NCAR 2 Reanalysis were retrieved from NOAA (https://psl.noaa.gov/data/gridded/data.ncep.reanalysis2.html), and Climate model outputs supplied by the Climate Variability Program Climate of the twentieth Century Plus Project (http://portal.nersc.gov/c20c/main.html).

Acknowledgments
The authors wish to acknowledge the Editor and the anonymous reviewers for their detailed and helpful comments to the original manuscript. This study was supported by the Second Tibetan Plateau Scientific Expedition and Research Program (STEP, Grant No. 2019QZKK0606), the National Natural Science Foundation of China (Grant No. 41621061), and by the National Key Research and Development Program—Global Change and Mitigation Project (Grant No. 2016YFA0602404). This work was also supported by a Swedish Research Council (2017-03780) and a Swedish Research Council for Sustainable Development (2019-00509) grant, and by the IBER-STILLING project, funded by the Spanish Ministry of Science, Innovation and Universities (RTI2018-095749-A-I00; MCIU/AEI/FEDER, UE).

References

Azorin-Molina, C., Dunn, R., Mears, C., Berrisford, P., Mcvicar, T., & Nicolas, J. P. (2019). Surface winds [in "State of the Climate in 2018"]. *Bulletin of the American Meteorological Society*, *100*(9), S43–S45.

Azorin-Molina, C., Guijarro, J.-A., McVicar, T. R., Vicente-Serrano, S. M., Chen, D., Jerez, S., & Espírito-Santo, F. (2016). Trends of daily peak wind gusts in Spain and Portugal, 1961–2014. *Journal of Geophysical Research: Atmospheres*, *121*(3), 1059–1078. https://doi.org/10.1002/2015jd024485

Azorin-Molina, C., Rehman, S., Guijarro, J. A., McVicar, T. R., Minola, L., Chen, D., & Vicente-Serrano, S. M. (2018). Recent trends in wind speed across Saudi Arabia, 1978–2013: A break in the stilling. *International Journal of Climatology*, *38*(S1), e966–e984. https://doi.org/10.1002/joc.5423

Azorin-Molina, C., Vicente-Serrano, S. M., Mcvicar, T. R., Jerez, S., Sanchez-Lorenzo, A., López-Moreno, J.-I., et al. (2014). Homogenization and assessment of observed near-surface wind speed trends over Spain and Portugal, 1961–2011. *Journal of Climate*, *27*(10), 3692–3712. https://doi.org/10.1175/jcli-d-13-00652.1

Bai, X., Shi, P., & Liu, Y. (2014). Society: Realizing China's urban dream. *Nature*, *509*(7499), 158–160. https://doi.org/10.1038/509158a

Bellprat, O., Guemas, V., Doblas-Reyes, F., & Donat, M. G. (2019). Towards reliable extreme weather and climate event attribution. *Nature Communications*, *10*(1), 1732. https://doi.org/10.1038/s41467-019-09729-2

Belušić Vozila, A., Güttler, I., Ahrens, B., Obermann-Hellhund, A., & Telišman Prtenjak, M. (2019). Wind over the Adriatic region in CORDEX climate change scenarios. *Journal of Geophysical Research: Atmosphere*, *124*(1), 110–130. https://doi.org/10.1029/2018JD028552

Branković, Č., Patarčić, M., Güttler, I., & Srnec, L. (2012). Near-future climate change over Europe with focus on Croatia in an ensemble of regional climate model simulations. *Climate Research*, *52*(1), 227–251. https://doi.org/10.3354/cr01058

Cai, W., Li, K., Liao, H., Wang, H., & Wu, L. (2017). Weather conditions conducive to Beijing severe haze more frequent under climate change. *Nature Climate Change*, *7*(4), 257–262. https://doi.org/10.1038/nclimate3249

Cai, W., Wang, G., Santoso, A., McPhaden, M. J., Wu, L., Jin, F.-F., et al. (2015). Increased frequency of extreme La Niña events under greenhouse warming. *Nature Climate Change*, *5*, 132. https://doi.org/10.1038/nclimate2492

Chen, H., & Wang, H. (2015). Haze days in North China and the associated atmospheric circulations based on daily visibility data from 1960 to 2012. *Journal of Geophysical Research: Atmospheres*, *120*(12), 5895–5909. https://doi.org/10.1002/2015jd023225

Chen, L., Li, D., & Pryor, S. C. (2013). Wind speed trends over China: Quantifying the magnitude and assessing causality. *International Journal of Climatology*, *33*(11), 2579–2590. https://doi.org/10.1002/joc.3613

Chen, L., Pryor, S. C., & Li, D. (2012). Assessing the performance of intergovernmental panel on climate change AR5 climate models in simulating and projecting wind speeds over China. *Journal of Geophysical Research*, *117*(D24), D24102. https://doi.org/10.1029/2012jd017533

Clifton, A., & Lundquist, J. K. (2012). Data clustering reveals climate impacts on local wind phenomena. *Journal of Applied Meteorology and Climatology*, *51*(8), 1547–1557. https://doi.org/10.1175/jamc-d-11-0227.1

Collins, M., An, S.-I., Cai, W., Ganachaud, A., Guilyardi, E., Jin, F.-F., et al. (2010). The impact of global warming on the tropical Pacific Ocean and El Niño. *Nature Geoscience*, *3*(6), 391–397. https://doi.org/10.1038/ngeo868

Dunn, R. J. H., Azorin-Molina, C., Mears, C. A., Berrisford, P., & McVicar, T. R. (2016). Global climate; atmospheric circulation surface winds [in "Stateof the Climate in 2015"]. *Bulletin of the American Meteorological Society*, *97*(8), S38–S40. https://doi.org/10.1175/2016BAMSStateoftheClimate.1

Gardiner, B., Berry, P., & Moulia, B. (2016). Review: Wind impacts on plant growth, mechanics and damage. *Plant Science*, *245*, 94–118. https://doi.org/10.1016/j.plantsci.2016.01.006

Gilbert, R. O. (1987). Sen's nonparametric estimator of slope. In. *Statistical methods for environmental pollution monitoring*. (pp. 217–219). Wiley.

Guijarro, J. A. (2017). Daily series homogenization and gridding with Climatol v.3. In. *Proceedings of Ninth Seminar for homogenization and quality control in climatological databases and fourth conference on spatial interpolation techniques in climatology and meteorology*. (pp. 175–180). Budapest, Hungary: World Meteorological Organization.

Güttler, I. (2011). Reducing warm bias over the north-eastern Europe in a regional climate model. *Croatian Meteorological Journal*, *44/45*, 19–29.

Han, Y. M., Han, Z. W., Cao, J. J., Chow, J. C., Watson, J. G., An, Z. S., et al. (2008). Distribution and origin of carbonaceous aerosol over a rural high-mountain lake area, Northern China and its transport significance. *Atmospheric Environment*, *42*(10), 2405–2414. https://doi.org/10.1016/j.atmosenv.2007.12.020

Hersbach, H., Bell, B., Berrisford, P., Hirahara, S., Horányi, A., Muñoz-Sabater, J., et al. (2020). The ERA5 global reanalysis. *Quarterly Journal of the Royal Meteorological Society*, *146*(730), 1999–2049. https://doi.org/10.1002/qj.3803

IPCC. (2013). *Climate Change 2013: The Physical Science Basis*. (p. 1535). Cambridge University Press. https://doi.org/10.1017/CBO9781107415324

Kalnay, E., Collins, W., Deaven, D., Gandin, L., Iredell, M., Jenne, R., & Joseph, D. (1996). The NCEP_NCAR 40-year reanalysis project. *Bulletin of the American Meteorological Society*, *77*(3), 437–472. https://doi.org/10.1175/1520-0477(1996)077<0437:TNYRP>2.0.CO;2

Kanamitsu, M., Ebisuzaki, W., Woollen, J., Yang, S.-K., Hnilo, J. J., Fiorino, M., & Potter, G. L. (2002). NCEP-DOE AMIP-II reanalysis (R-2). *Bulletin of the American Meteorological Society*, *83*, 1631–1643. https://doi.org/10.1175/bams-83-11-1631(2002)083<1631:nar>2.3.co;2

Karnauskas, K. B., Lundquist, J. K., & Zhang, L. (2018). Southward shift of the global wind energy resource under high carbon dioxide emissions. *Nature Geoscience*, *11*(1), 38–43. https://doi.org/10.1038/s41561-017-0029-9

Kendall, M. G., & Gibbons, J. D. (1990). *Rank correlation methods*. (p. 272). Oxford University Press.

Kim, J. C., & Paik, K. (2015). Recent recovery of surface wind speed after decadal decrease: A focus on South Korea. *Climate Dynamics*, *45*(5–6), 1699–1712. https://doi.org/10.1007/s00382-015-2546-9

Kosaka, Y., & Xie, S.-P. (2013). Recent global-warming hiatus tied to equatorial Pacific surface cooling. *Nature*, *501*, 403. https://doi.org/10.1038/nature12534

Li, J., Ma, X., & Zhang, C. (2020). Predicting the spatiotemporal variation in soil wind erosion across Central Asia in response to climate change in the 21st century. *Science of the Total Environment*, *709*, 136060. https://doi.org/10.1016/j.scitotenv.2019.136060

Li, J., Wu, Z., Jiang, Z., & He, J. (2010). Can global warming strengthen the East Asian summer monsoon? *Journal of Climate*, *23*(24), 6696–6705. https://doi.org/10.1175/2010jcli3434.1

Li, Y., Chen, Y., Li, Z., & Fang, G. (2018). Recent recovery of surface wind speed in northwest China. *International Journal of Climatology*, *38*(12), 4445–4458. https://doi.org/10.1002/joc.5679

Li, Z., Song, L., Ma, H., Xiao, J., Wang, K., & Chen, L. (2018). Observed surface wind speed declining induced by urbanization in East China. *Climate Dynamics*, *50*(3–4), 735–749. https://doi.org/10.1007/s00382-017-3637-6

Lin, C., Yang, K., Huang, J., Tang, W., Qin, J., Niu, X., et al. (2015). Impacts of wind stilling on solar radiation variability in China. *Scientific Reports*, *5*, 1–7. https://doi.org/10.1038/srep15135

Lin, C., Yang, K., Qin, J., & Fu, R. (2013). Observed coherent trends of surface and upper-air wind speed over China since 1960. *Journal of Climate*, *26*(9), 2891–2903. https://doi.org/10.1175/jcli-d-12-00093.1

Lindsay, R., Wensnahan, M., Schweiger, A., & Zhang, J. (2014). Evaluation of seven different atmospheric reanalysis products in the Arctic. *Journal of Climate*, *27*(7), 2588–2606. https://doi.org/10.1175/jcli-d-13-00014.1

McVicar, T. R., Roderick, M. L., Donohue, R. J., Li, L. T., Van Niel, T. G., Thomas, A., et al. (2012). Global review and synthesis of trends in observed terrestrial near-surface wind speeds: Implications for evaporation. *Journal of Hydrology*, *416–417*, 182–205. https://doi.org/10.1016/j.jhydrol.2011.10.024

McVicar, T. R., Van Niel, T. G., Li, L. T., Roderick, M. L., Rayner, D. P., Ricciardulli, L., & Donohue, R. J. (2008). Wind speed climatology and trends for Australia, 1975–2006: Capturing the stilling phenomenon and comparison with near-surface reanalysis output. *Geophysical Research Letters*, *35*(20), 1–6. https://doi.org/10.1029/2008gl035627

McVicar, T. R., Van Niel, T. G., Roderick, M. L., Li, L. T., Mo, X. G., Zimmermann, N. E., & Schmatz, D. R. (2010). Observational evidence from two mountainous regions that near-surface wind speeds are declining more rapidly at higher elevations than lower elevations: 1960–2006. *Geophysical Research Letters*, *37*(6), 1–6. https://doi.org/10.1029/2009gl042255

Minola, L., Azorin-Molina, C., & Chen, D. (2016). Homogenization and assessment of observed near-surface wind speed trends across Sweden, 1956–2013. *Journal of Climate*, *29*(20), 7397–7415. https://doi.org/10.1175/jcli-d-15-0636.1

Minola, L., Zhang, F., Azorin-Molina, C., Pirooz, A. A. S., Flay, R. G. J., Hersbach, H., & Chen, D. (2020). Near-surface mean and gust wind speeds in ERA5 across Sweden: Towards an improved gust parametrization. *Climate Dynamics*, *55*(3–4), 887–907. https://doi.org/10.1007/s00382-020-05302-6

Moemken, J., Reyers, M., Feldmann, H., & Pinto, J. G. (2018). Future changes of wind speed and wind energy potentials in EURO-CORDEX ensemble simulations. *Journal of Geophysical Research: Atmospheres*, *123*(12), 6373–6389. https://doi.org/10.1029/2018jd028473

Neumayer, E., Plümper, T., & Barthel, F. (2014). The political economy of natural disaster damage. *Global Environmental Change*, *24*, 8–19. https://doi.org/10.1016/j.gloenvcha.2013.03.011

Peng, D., Zhou, T., Zhang, L., & Wu, B. (2018). Human contribution to the increasing summer precipitation in Central Asia from 1961 to 2013. *Journal of Climate*, *31*(19), 8005–8021. https://doi.org/10.1175/jcli-d-17-0843.1

Peters, G. P., Andrew, R. M., Canadell, J. G., Fuss, S., Jackson, R. B., Korsbakken, J. I., et al. (2017). Key indicators to track current progress and future ambition of the Paris Agreement. *Nature Climate Change*, *7*, 118. Retrieved from: https://doi.org/10.1038/nclimate3202

Piao, S., Yin, G., Tan, J., Cheng, L., Huang, M., Li, Y., et al. (2015). Detection and attribution of vegetation greening trend in China over the last 30 years. *Global Change Biology*, *21*(4), 1601–1609. https://doi.org/10.1111/gcb.12795

Pirazzoli, P. A., & Tomasin, A. (2003). Recent near-surface wind changes in the central Mediterranean and Adriatic areas. *International Journal of Climatology*, *23*(8), 963–973. https://doi.org/10.1002/joc.925

Pryor, S. C., Barthelmie, R. J., Young, D. T., Takle, E. S., Arritt, R. W., Flory, D., et al. (2009). Wind speed trends over the contiguous United States. *Journal of Geophysical Research*, *114*, D14105. https://doi.org/10.1029/2008jd011416

Roderick, M. L., Rotstayn, L. D., Farquhar, G. D., & Hobbins, M. T. (2007). On the attribution of changing pan evaporation. *Geophysical Research Letters*, *34*(17), 1–6. https://doi.org/10.1029/2007gl031166

Rogelj, J., den Elzen, M., Höhne, N., Fransen, T., Fekete, H., Winkler, H., et al. (2016). Paris Agreement climate proposals need a boost to keep warming well below 2°C. *Nature*, *534*, 631. https://doi.org/10.1038/nature18307

Segovia, C., Gómez, J. D., Gallardo, P., Lozano, F. J., & Asensio, C. (2017). Soil nutrients losses by wind erosion in a citrus crop at southeast Spain. *Eurasian Soil Science*, *50*(6), 756–763. https://doi.org/10.1134/s1064229317060114

Shi, P., Zhang, G., Kong, F., Chen, D., Azorin-Molina, C., & Guijarro, J. A. (2019). Variability of winter haze over the Beijing-Tianjin-Hebei region tied to wind speed in the lower troposphere and particulate sources. *Atmospheric Research*, *215*, 1–11. https://doi.org/10.1016/j.atmosres.2018.08.013

Shi, P.-J., Zhang, G.-F., Kong, F., & Ye, Q. (2015). Wind speed change regionalization in China (1961–2012). *Advances in Climate Change Research*, *6*(2), 151–158. https://doi.org/10.1016/j.accre.2015.09.006

Stone, D. A., Christidis, N., Folland, C., Perkins-Kirkpatrick, S., Perlwitz, J., Shiogama, H., et al. (2019). Experiment design of the International CLIVAR C20C+ Detection and Attribution project. *Weather and Climate Extremes*, *24*, 100206. https://doi.org/10.1016/j.wace.2019.100206

Tobin, I., Berrisford, P., Dunn, R. J. H., Vautard, R., & McVicar, T. R. (2014). Global climate: Atmospheric circulation and land surface wind speed [in "State of the Climate in 2013"]. *Bulletin of the American Meteorological Society*, *95*(7), S28–S29. https://doi.org/10.1175/2014BAMSStateoftheClimate.1

Vautard, R., Cattiaux, J., Yiou, P., Thépaut, J.-N., & Ciais, P. (2010). Northern Hemisphere atmospheric stilling partly attributed to an increase in surface roughness. *Nature Geoscience*, *3*(11), 756–761. https://doi.org/10.1038/ngeo979

Vautard, R., Thais, F., Tobin, I., Bréon, F.-M., de Lavergne, J.-G. D., Colette, A., et al. (2014). Regional climate model simulations indicate limited climatic impacts by operational and planned European wind farms. *Nature Communications*, *5*(1), 3196. https://doi.org/10.1038/ncomms4196

Wan, H., Wang, X. L., & Swail, V. R. (2010). Homogenization and trend analysis of Canadian near-surface wind speeds. *Journal of Climate*, *23*(5), 1209–1225. https://doi.org/10.1175/2009jcli3200.1

Wang, H., He, S., & Liu, J. (2013). Present and future relationship between the East Asian winter monsoon and ENSO: Results of CMIP5. *Journal of Geophysical Research: Oceans*, *118*(10), 5222–5237. https://doi.org/10.1002/jgrc.20332

Wang, R., Liu, B., Li, H., Zou, X., Wang, J., Liu, W., et al. (2017). Variation of strong dust storm events in northern China during 1978–2007. *Atmospheric Research*, *183*, 166–172. https://doi.org/10.1016/j.atmosres.2016.09.002

Watanabe, M., Shiogama, H., Tatebe, H., Hayashi, M., Ishii, M., & Kimoto, M. (2014). Contribution of natural decadal variability to global warming acceleration and hiatus. *Nature Climate Change*, *4*, 893. Retrieved from: https://doi.org/10.1038/nclimate2355

Weatherhead, E. C., Reinsel, G. C., Tiao, G. C., Meng, X.-L., Choi, D., Cheang, W.-K., et al. (1998). Factors affecting the detection of trends: Statistical considerations and applications to environmental data. *Journal of Geophysical Research*, *103*(D14), 17149–17161. https://doi.org/10.1029/98jd00995

Wever, N. (2012). Quantifying trends in surface roughness and the effect on surface wind speed observations. *Journal of Geophysical Research*, *117*(11), 1–14. https://doi.org/10.1029/2011jd017118

Wohland, J., Omrani, N. E., Witthaut, D., & Keenlyside, N. S. (2019). Inconsistent wind speed trends in current twentieth century reanalyses. *Journal of Geophysical Research: Atmospheres*, *124*(4), 1931–1940. https://doi.org/10.1029/2018jd030083

Wu, J., Zha, J., Zhao, D., & Yang, Q. (2018). Changes in terrestrial near-surface wind speed and their possible causes: An overview. *Climate dynamics*, *51*. https://doi.org/10.1007/s00382-017-3997-y

Xu, B., Gu, Z., Wang, L., Hao, Q., Wang, H., Chu, G., et al. (2019). Global warming increases the incidence of haze days in China. *Journal of Geophysical Research: Atmospheres*, *124*, 6180–6190. https://doi.org/10.1029/2018jd030119

Xu, M., Chang, C.-P., Fu, C., Qi, Y., Robock, A., Robinson, D., & Zhang, H. (2006). Steady decline of east Asian monsoon winds, 1969–2000: Evidence from direct ground measurements of wind speed. *Journal of Geophysical Research*, *111*(D24), D24111. https://doi.org/10.1029/2006jd007337

Xu, Z., & Yang, Z. L. (2015). A new dynamical downscaling approach with GCM bias corrections and spectral nudging. *Journal of Geophysical Research: Atmospheres*, *120*(8), 3063–3084. https://doi.org/10.1002/2014jd022958

Yao, S.-L., Luo, J.-J., Huang, G., & Wang, P. (2017). Distinct global warming rates tied to multiple ocean surface temperature changes. *Nature Climate Change*, *7*, 486. Retrieved from: https://doi.org/10.1038/nclimate3304

You, Q., Fraedrich, K., Min, J., Kang, S., Zhu, X., Pepin, N., & Zhang, L. (2014). Observed surface wind speed in the Tibetan Plateau since 1980 and its physical causes. *International Journal of Climatology*, *34*(6), 1873–1882. https://doi.org/10.1002/joc.3807

Zeng, Z., Ziegler, A. D., Searchinger, T., Yang, L., Chen, A., Ju, K., et al. (2019). A reversal in global terrestrial stilling and its implications for wind energy production. *Nature Climate Change*, *9*(12), 979–985. https://doi.org/10.1038/s41558-019-0622-6

Zhang, G., Azorin-Molina, C., Chen, D., Guijarro, J. A., Kong, F., Minola, L., et al. (2020). Variability of daily maximum wind speed across China, 1975–2016: An examination of likely causes. *Journal of Climate*, *33*(7), 2793–2816. https://doi.org/10.1175/jcli-d-19-0603.1

Zhang, G., Azorin-Molina, C., Shi, P., Lin, D., Guijarro, J. A., Kong, F., & Chen, D. (2019). Impact of near-surface wind speed variability on wind erosion in the eastern agro-pastoral transitional zone of Northern China, 1982–2016. *Agricultural and Forest Meteorology*, *271*, 102–115. https://doi.org/10.1016/j.agrformet.2019.02.039

Zhang, R., Zhang, S., Luo, J., Han, Y., & Zhang, J. (2019). Analysis of near-surface wind speed change in China during 1958–2015. *Theoretical and Applied Climatology*, *137*, 2785–2801. https://doi.org/10.1007/s00704-019-02769-0

Zhang, Z., Wang, K., Chen, D., Li, J., & Dickinson, R. (2019). Increase in surface friction dominates the observed surface wind speed decline during 1973–2014 in the Northern Hemisphere lands. *Journal of Climate*, *32*(21), 7421–7435. https://doi.org/10.1175/jcli-d-18-0691.1

Zhang, Z., Zhang, X., Gong, D., Kim, S.-J., Mao, R., & Zhao, X. (2016). Possible influence of atmospheric circulations on winter haze pollution in the Beijing-Tianjin-Hebei region, northern China. *Atmospheric Chemistry and Physics*, *16*(2), 561–571. https://doi.org/10.5194/acp-16-561-2016

Zhu, C., Wang, B., Qian, W., & Zhang, B. (2012). Recent weakening of northern East Asian summer monsoon: A possible response to global warming. *Geophysical Research Letters*, *39*(9), 1–6. https://doi.org/10.1029/2012gl051155

Zhu, Z., Piao, S., Myneni, R. B., Huang, M., Zeng, Z., Canadell, J. G., et al. (2016). Greening of the Earth and its drivers. *Nature Climate Change*, *6*(8), 791–795. https://doi.org/10.1038/nclimate3004